Cell Reports

Article

Insulin and serine metabolism as sex-specific hallmarks of Alzheimer's disease in the human hippocampus

Graphical abstract

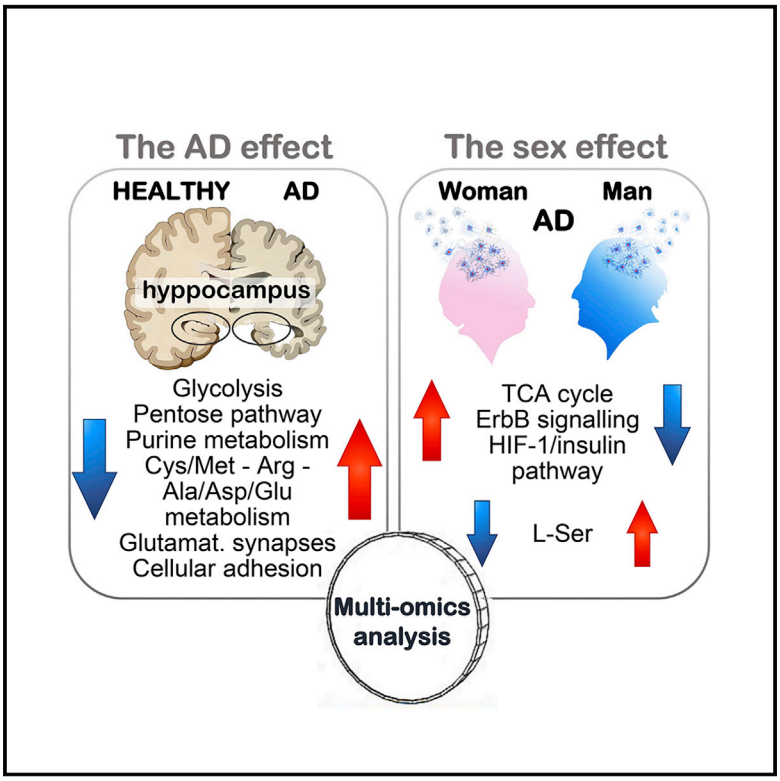

Highlights

- Multi-omics analysis identified sex-specific AD hallmarks in human hippocampus
- D-Ser/total Ser ratio increases in the hippocampus of women with AD
- The insulin pathway decreases in women compared with men with AD
- The alterations in Arg and Ala/Asp/Glu metabolism in AD are not sex specific

Authors

Elisa Maffioli, Giulia Murtas, Valentina Rabattoni, ..., Gabriella Tedeschi, Paola Coccetti, Loredano Pollegioni

Correspondence

nadia.canu@uniroma2.it (N.C.), gabriella.tedeschi@unimi.it (G.T.), paola.coccetti@unimib.it (P.C.), loredano.pollegioni@uninsubria.it (L.P.)

In brief

Maffioli et al. perform a multi-omics analysis of the hippocampus of individuals with Alzheimer's disease (AD) and healthy controls. Considering the sex of the individuals, women with AD display a decrease in the insulin response and an increase in the D-serine/total serine ratio compared with men with AD.

Maffioli et al., 2022, Cell Reports *40*, 111271
September 6, 2022
https://doi.org/10.1016/j.celrep.2022.111271

CellPress

Cell Reports

CellPress
OPEN ACCESS

Article

Insulin and serine metabolism as sex-specific hallmarks of Alzheimer's disease in the human hippocampus

Elisa Maffioli,[1,2,9] Giulia Murtas,[3,9] Valentina Rabattoni,[3,9] Beatrice Badone,[4,8] Farida Tripodi,[4] Filomena Iannuzzi,[5] Danilo Licastro,[6] Simona Nonnis,[1,2] Anna Maria Rinaldi,[5] Zoraide Motta,[3] Silvia Sacchi,[3,10] Nadia Canu,[5,7,*] Gabriella Tedeschi,[1,2,*] Paola Coccetti,[4,*] and Loredano Pollegioni[3,*]

[1]DIVAS, Department of Veterinary Medicine and Animal Science, University of Milano, 20121 Milano, Italy
[2]CIMAINA, University of Milano, 20121 Milano, Italy
[3]Department of Biotechnology and Life Sciences, University of Insubria, 21100 Varese, Italy
[4]Department of Biotechnology and Biosciences, University of Milano-Bicocca, 20126 Milano, Italy
[5]Department of System Medicine, University of Rome "Tor Vergata," 00133 Rome, Italy
[6]Area Science Park, Basovizza, 34149 Trieste, Italy
[7]Istituto di Biochimica e Biologia Cellulare (IBBC) CNR, 00015 Monterotondo Scalo, Italy
[8]Present address: Sophion Bioscience A/S, Baltorpvej 154, 2750 Ballerup, Denmark
[9]These authors contributed equally
[10]Lead contact
*Correspondence: nadia.canu@uniroma2.it (N.C.), gabriella.tedeschi@unimi.it (G.T.), paola.coccetti@unimib.it (P.C.), loredano.pollegioni@uninsubria.it (L.P.)
https://doi.org/10.1016/j.celrep.2022.111271

SUMMARY

Healthy aging is an ambitious aspiration for humans, but neurodegenerative disorders, such as Alzheimer's disease (AD), strongly affect quality of life. Using an integrated omics approach, we investigate alterations in the molecular composition of postmortem hippocampus samples of healthy persons and individuals with AD. Profound differences are apparent between control and AD male and female cohorts in terms of up- and downregulated metabolic pathways. A decrease in the insulin response is evident in AD when comparing the female with the male group. The serine metabolism (linked to the glycolytic pathway and generating the N-methyl-D-aspartate [NMDA] receptor coagonist D-serine) is also significantly modulated: the D-Ser/total serine ratio represents a way to counteract age-related cognitive decline in healthy men and during AD onset in women. These results show how AD changes and, in certain respects, almost reverses sex-specific proteomic and metabolomic profiles, highlighting how different pathophysiological mechanisms are active in men and women.

INTRODUCTION

Sporadic and late-onset Alzheimer's disease (AD), the major contributor to dementia worldwide (World Alzheimer Report 2019, available at https://www.alz.co.uk/research/world-report-2019), is an age-dependent neurodegenerative disorder affecting different brain regions, in particular the hippocampus, an area that is critical for learning and memory (Kapogiannis and Mattson, 2011). Although the specific cause of AD is unknown, the greatest risk factors are genetic background, environment, dysfunctional glucose metabolism associated with oxidative stress and neuroinflammation, and sex (Podcasy and Epperson, 2016; Butterfield and Halliwell, 2019; Arnold et al., 2020). Compared with men, women are at increased risk for AD because of their longer life expectancy, worse consequences linked to APOE4 expression (Altmann et al., 2014; Gamache et al., 2020), and the decline in estrogen levels at menopause (Podcasy and Epperson, 2016; Arnold et al., 2020). In individuals with AD, glucose hypometabolism, which occurs before symptoms or pathology become manifest (Sposato et al., 2019), activates feedback loops that perturb various metabolic pathways essential for neuronal homeostasis and neurotransmission (Daulatzai, 2017), contributing to neurodegeneration. Alterations of glycolysis and the tricarboxylic acid (TCA) cycle have an effect on acetyl-coenzyme A (CoA) metabolism, which strictly correlates with reported reduced energy production in mitochondria and impaired cholinergic neurotransmission (because of the reduction of acetylcholine synthesis) in AD (Szutowicz et al., 2013; Paglia et al., 2016).

Intimately connected to glucose metabolism is L-serine (L-Ser), which is classified as a nutritional nonessential amino acid for humans and animals. L-Ser is required in protein synthesis, functioning as a precursor of other nonessential amino acids (glycine [Gly] and cysteine [Cys]) and of phosphatidylserine, and is needed for ceramide synthesis; it also provides carbons for synthesis of glutathione (GSH) and reduced nicotinamide adenine dinucleotide phosphate (NADPH) via

its conversion into Gly in astrocytes (Fan et al., 2014) and feeds folate and methionine cycles. The latter two cycles represent pathways related to one-carbon metabolism, which generates building blocks for new cellular components; e.g., purine and thymidine. L-Ser is present in the blood, and it diffuses poorly through the blood-brain barrier, at rates ~5–7 times lower than other amino acids (Oldendorf, 1971). In the brain, L-Ser is produced *de novo* from the glycolytic intermediate 3-phosphoglycerate (3PG) through the cytosolic "phosphorylated pathway" (PP), which involves three enzymes: 3PG dehydrogenase (PHGDH), phosphoserine aminotransferase (PSAT), and phosphoserine phosphatase (PSP) (Murtas et al., 2020). The PP plays a critical role in the brain, controlling L-Ser production and using/producing central metabolites and cofactors (glutamate [Glu], 2-ketoglutarate, and reduced/oxidised ratio of nicotinamide adenine dinucleotide [NADH/NAD^+]). In the brain, L-Ser is mainly synthesized in glial cells (Murtas et al., 2020; Maugard et al., 2021), and the amino acid transporter ASC1 mediates shuttling of this amino acid to neurons (Wolosker, 2011; Neame et al., 2019).

L-Ser is also the precursor of two molecules that regulate excitatory glutamatergic transmission: D-Ser and Gly. D-Ser is the main coagonist of synaptic N-methyl-D-aspartate (NMDA) receptors (NMDARs) in the hippocampus, and Gly plays the same role at extrasynaptic sites (Papouin et al., 2012) and acts as an inhibitory neurotransmitter via ionotropic Gly receptors. Because the coagonist binding site of NMDAR is not saturated *in vivo,* a tiny change in D-Ser levels can dynamically modulate receptor responses, including synaptic transmission and plasticity. NMDAR signaling levels, which must be balanced to promote neuronal survival and prevent neurodegeneration, are known to be altered in AD (Paula-Lima et al., 2013; Armada-Moreira et al., 2020). NMDAR neurotransmission can be controlled by acting on metabolism and availability of D-Ser; brain-produced L-Ser is converted into the D-enantiomer by Ser racemase (SR or SRR) mainly in neurons and shuttled to astrocytes, where it is degraded by SR and D-amino acid oxidase (DAAO or DAO) (Pollegioni and Sacchi, 2010; Wolosker, 2011). NMDAR activation by D-Ser and Gly might also be regulated by the PP (Neame et al., 2019), and various Ser synthesis disorders because of mutations in the enzymes of the PP have been identified in individuals with neurological symptoms (Shaheen et al., 2014; Murtas et al., 2021). *PHGDH* is the only gene found to be consistently upregulated in transcriptomes from five brain regions (temporal cortex, dorsolateral prefrontal cortex, superior temporal gyrus, parahippocampal gyrus, and inferior frontal gyrus) of individuals with AD (Yan et al., 2020). Additional amino acids are related to neurotransmission and AD onset. For example, arginine (Arg) levels and signaling are involved in inhibitory and excitatory neurotransmission via adenosine and other metabolites, in maintaining microtubule stability, in degrading protein aggregates (Savarin et al., 2010; Hunt et al., 2015), in β-amyloid deposition and microglial activation (Ma et al., 2021), and in tau aggregation (Sandusky-Beltran et al., 2021).

Here we evaluated the alterations observed in hippocampal regions of individuals with AD compared with healthy individuals by using a multi-omics approach, focusing on the relevant pathways related to Ser metabolism and on the sex effect.

RESULTS

Altered transcriptomics profile of hippocampal tissues in individuals with AD: Sex has a main effect

We examined the transcriptomics profile of the hippocampus in a cohort of 21 individuals affected by AD and 19 cognitively normal controls (see Table S1 for clinical pathological information about samples). Analysis of differentially expressed genes by DeqSeq2 identified a total of 476 differentially expressed genes (DEGs) (p adjusted $\leq$ 0.05) between AD individuals and controls: 204 were upregulated, and 272 were downregulated. Differentially expressed protein-coding genes account for 76% of upregulated and 69% of downregulated genes, with the remaining being long non-coding RNA (lncRNA) (Figures 1A and 1B).

To compare our transcriptome analysis with the recently and comprehensive transcriptome investigation performed on hippocampal samples from a large cohort of individuals with AD (Crist et al., 2021) and with single-cell RNA analysis performed in the prefrontal cortex (PFC) during AD progression (Mathys et al., 2019), a rotation gene set test based on the tables of DEGs available in the two reported studies was performed. From both studies, only tables related to our biological question were selected; almost all genes reported (>93%) were detected in our RNA sequencing (RNA-seq) experiment too (Table S2; Figure S1). The analysis shows a significant enrichment for the hippocampal sample dataset as well as for astrocytes and inhibitory neurons of the single-cell RNA dataset, suggesting results compatible with the related tables of the selected publications.

DEG (p < 0.05) over-representation analysis (ORA) using the ConsensusPathDB (http://cpdb.molgen.mpg.de/CPDB/tutorial#moreinfo.discl) identified several pathways enriched in the AD dataset compared with control (CTR) samples, which have been reported previously to be affected in AD (Cortes-Canteli et al., 2015; van Rooij et al., 2019). These pathways include calcineurin-dependent nuclear factor of activated T cells (NFAT) signaling (Kipanyula et al., 2016), bile acid and bile salt signaling, insulin-mediated glucose transport and γ-aminobutyric acid (GABA) synthesis, and amino acid metabolism (Gly, Ser, Ala, Pro, Thr, and Asp) (Griffin and Bradshaw, 2017; Table S3A). These findings have been largely confirmed by ingenuity pathway analysis (IPA) of the canonical pathways associated with DEGs identified in our AD samples (Figure 1C; Table S3A). Two of the enriched pathways linked to cholesterol metabolism/clearance and neuroinflammation (atherosclerosis signaling and bile acid and salt biosynthesis) are known to be altered in the brain of individuals with AD and contribute to cognitive decline (Baloni et al., 2020; Gamba et al., 2021). The most significantly upregulated genes associated with the atherosclerosis pathway were the ones encoding the lipoxygenase ALOX15 and chemokine receptor 4 (CRCX4), which were found in cell types that mediate inflammation in the brain, such as microglia, and are involved in plaque formation in arteries. This latter process, like that implicated in tau and amyloid buildup in AD (Sergin et al., 2016), is the main cause of cerebral hypoperfusion and the ensuing oxidative stress (Polis and Samson, 2019). IPA predicted a

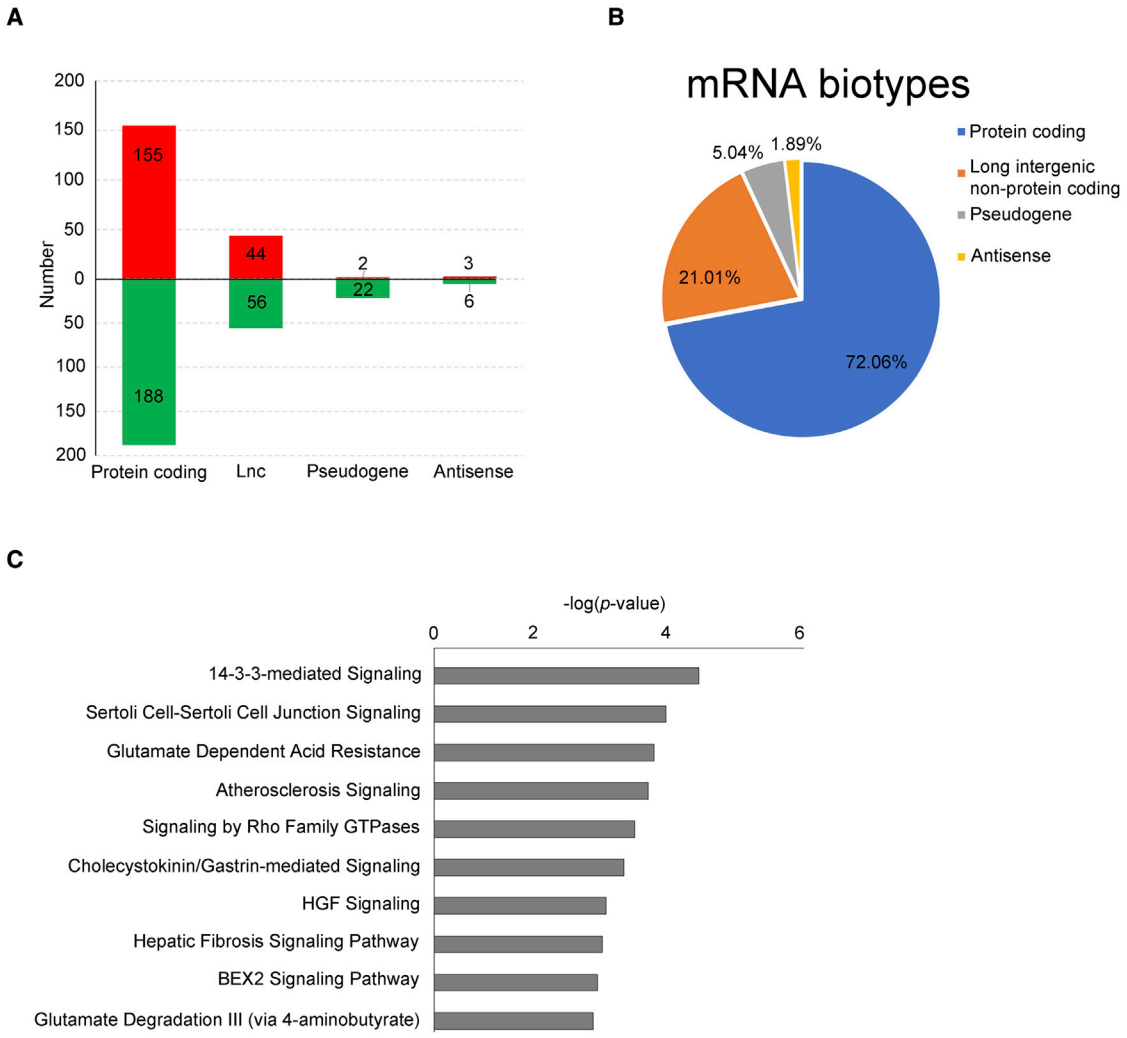

Figure 1. Distribution of significant DEGs (false discovery rate [FDR]-adjusted p $\leq$ 0.05) between AD and CTRs

(A) The proportion of upregulated genes is represented in green, and downregulated genes are represented in red. The total number of significant DEGs is provided on each bar.

(B) Pie chart of DEG biotype classification based on Ingenuity annotation.

(C) Top 10 canonical pathways obtained from Ingenuity analysis of the downregulated protein-coding genes in late-onset AD hippocampus. Each bar represents the score (-log p value) obtained for the ORA. The full list of pathways is available in Table S3A.

nondirectional protein interaction map in the form of networks with associated functions, including those linked to neurological diseases (as expected), tissue development, cell-to-cell signaling and interaction, organismal injury, and cellular assembly and organization (Table S3A). Analysis of these networks supports the heterogeneous nature of AD, highlighting various pathophysiological mechanisms beyond the typical dogma of β-amyloid cascade and tau pathology (Neff et al., 2021).

To test the effect of sex on our transcriptomics dataset, healthy male CTRs (CTRM; n = 9) and female CTRs (CTRF; n = 10) were compared. ORA identified the most enriched pathways related to this comparison, among which were aminoacyl-tRNA biosynthesis, the TCA cycle and respiratory electron transport, and thermogenesis (Table S3B). The top networks identified by IPA are related to molecular transport, cancer, cell development, and cell-to-cell signaling. Focusing on female samples, from IPA of DEGs in AD females (ADF) (n = 10) versus CTRF (n = 10), many pathways were downregulated, in particular amyotrophic lateral sclerosis signaling, mitogen-associated protein kinase (MAPK), epidermal growth factor (EGF), and erythroblastic leukemia viral oncogene homolog (ErbB) signaling, 14-3-3-mediated signaling, and unfolded protein response (Table S3C shows the complete IPA, including the main networks activated). As concerns men, among the DEGs regulated between AD males (ADM) (n = 11) versus CTRM (n = 9), many were lncRNAs and antisense RNAs. The main top networks involved are related to glucocorticoid receptor signaling, protein ubiquitination, HIF1α signaling, and androgen and aldosterone signaling (see IPA in Table S3D). Network analysis identified neurological diseases and free radical scavenging networks. Increasing evidence

suggests that oxidative stress has a key role in late-onset sporadic forms, which are the majority of AD cases (Tönnies and Trushina, 2017). Finally, the effect of sex on the transcriptomics profile in AD was also evident by comparing ADF (n = 10) and ADM (n = 11) (Table S3E). ORA showed that the most enriched pathways were related to chromatin modification and organization, suggesting a main epigenomic effect at the transcriptomic level between male and female hippocampus samples in AD.

Our transcriptional analysis compares well with a previous large cohort of hippocampal AD samples (Crist et al., 2021), highlights selected pathways altered differently in AD versus healthy CTRs, and suggests a main effect of sex in physiological aging and pathological AD.

Proteome analyses of hippocampal tissues: Effect of AD and sex

To analyze the alterations in the hippocampal proteome associated with AD, a quantitative shotgun, label-free strategy was applied (Table S1). The analysis highlighted significant differences between AD (n = 23) and CTR (n = 20) samples (Figures S2A and S2B; Table S4A). Bioinformatics analysis by ClueGo on the differentially expressed proteins (DEPs) showed that almost 57% of the terms enriched in AD samples were related to metabolic processes, confirming the profound involvement of cell metabolism in this neurological disorder (Figure S2C; Tables S4B–S4D). Other factors known to be heavily altered in AD, such as cytoskeleton, transport, neuronal system, axon guidance, and synapse organization, were among the most decreased terms in AD samples, in accordance with most of the data reported so far in the literature (Rayaprolu et al., 2021). The results from the David and Panther programs confirmed this trend (Tables S4C and S4D), well in accordance with the finding by Johnson et al. (2020), who carried out a large-scale proteomics analysis of AD brains (dorsolateral PFC) and highlighted the importance of inflammation, sugar metabolism, mitochondrial function, synaptic function, RNA-associated proteins, and glia in the pathogenesis of AD.

We compared the proteomics profiles of hippocampal tissues according to sex in affected individuals and healthy subjects. By comparing CTRM (n = 9) and CTRF (n = 10), the analysis revealed an evident separation of the sexes (Figures 2A, S2A, and S2C; Table S5A). Multiple analyses by ClueGo, David, and Panther identified the most enriched pathways among the differentially abundant proteins in each group, suggesting significant enrichment in proteins related to membrane trafficking, neutrophil degranulation, lipid metabolism, amino acid metabolism, Cys/Met metabolism, and response to oxidative stress in CTRFs, whereas vesicle transport, axon guidance, synaptic transmission, neurotransmitter secretion, amino acids transport, and activation of various receptors were prevalent in CTRMs (Figure 2A; Tables S4 and S5).

Based on these findings, sex separation was taken into account, focusing on specific comparisons (i.e., ADF versus CTRF, ADM versus CTRM, and ADF versus ADM); a summary of the results is reported in Figures 3A and S2C, and Tables S5B–S5D list the DEPs or the ones exclusively expressed in one condition of these three comparisons (the corresponding volcano plots are shown in Figure S2B).

Differential protein expression in ADF in comparison to CTRF strongly suggests a cell response to oxidative stress and inflammatory conditions, increase in aggrephagy (Figure S2C; Table S4), and significant alteration of intracellular cytosolic trafficking, secretion, membrane fusion, cytoskeleton organization, and cell adhesion pathways, which are also increased. There is a decrease in chemokine- and cytokine-mediated inflammation (Table S4D). Proteins involved in synaptic transmission, Golgi apparatus-to-endoplasmic reticulum (ER) transport, protein folding and localization, membrane trafficking, axon guidance, microtubule and, above all, organelle organization were decreased (Figure S2C; Table S4B), pointing to alterations in the complex interplay between fusion and fission in mitochondria and the ER and suggesting that removal of damaged organelles is compromised, as are quality, bioenergetic capacity, and mitochondrial homeostasis (Flannery and Trushina, 2019).

In men, terms referring to metabolic alterations were prevalent in AD in comparison with CTRs. Ser family amino acid metabolic process, Cys, Met, GSH, and other amino acid metabolisms constitute 53.17% of the terms enriched in ADM (Figure S2C; Tables S4B and S4D). Vesicle-mediated transport and establishment of cell localization were increased. Modulation of peroxisome proliferation-activated receptor (PPAR) signaling, which controls expression of genes involved in adipogenesis, lipid metabolism, inflammation, and maintenance of metabolic homeostasis, and a reduction of the TCA cycle, lipid catabolism, and aerobic respiration were additional pathways identified by bioinformatics analysis of ADM versus CTRM.

The effect of sex on the proteomics pattern in AD was also evident by comparing ADF and ADM samples. Cadherin binding, cellular response to hypoxia and stress, axon guidance, nervous system development, protein localization to the ER, and amino acid metabolism were mainly increased in ADF in comparison with ADM; Glu NMDAR activation, regulation of insulin secretion, neuron projection, morphogenesis, endocytosis and mitochondrial protein import, synapses, and bone development were prevalent in ADM (Figures 3 and S5; Tables S4B–S4D and S5D).

Metabolomics profile of hippocampal tissues: Sex differences between CTRs and AD

Given the high number of DEPs involved in metabolic processes (Figures 2A and 3A), we explored the metabolome of healthy and AD-affected individuals by performing an untargeted metabolomics analysis on the same hippocampal samples. When comparing CTR (n = 20) and AD (n = 23) samples (Table S1), separated profiles were apparent according to partial least-squares discriminant analysis (PLS-DA) (Figure S3A); of 126 metabolites detected, 13 and 11 were up- and downregulated, respectively (Table S6). Set enrichment analysis revealed that the most significantly upregulated pathways in AD samples were Arg/Pro metabolism and the pentose phosphate pathway (PPP) (Figure S3B). In contrast, the most significantly downregulated ones in AD samples were Ala/Asp/Glu metabolism, pyruvate metabolism, glycolysis/gluconeogenesis, pyrimidine metabolism, and aminoacyl-tRNA biosynthesis (Figure S3B; Table S6). Arg and the PPP were among the most enriched pathways altered in the plasma of individuals with AD as well as of

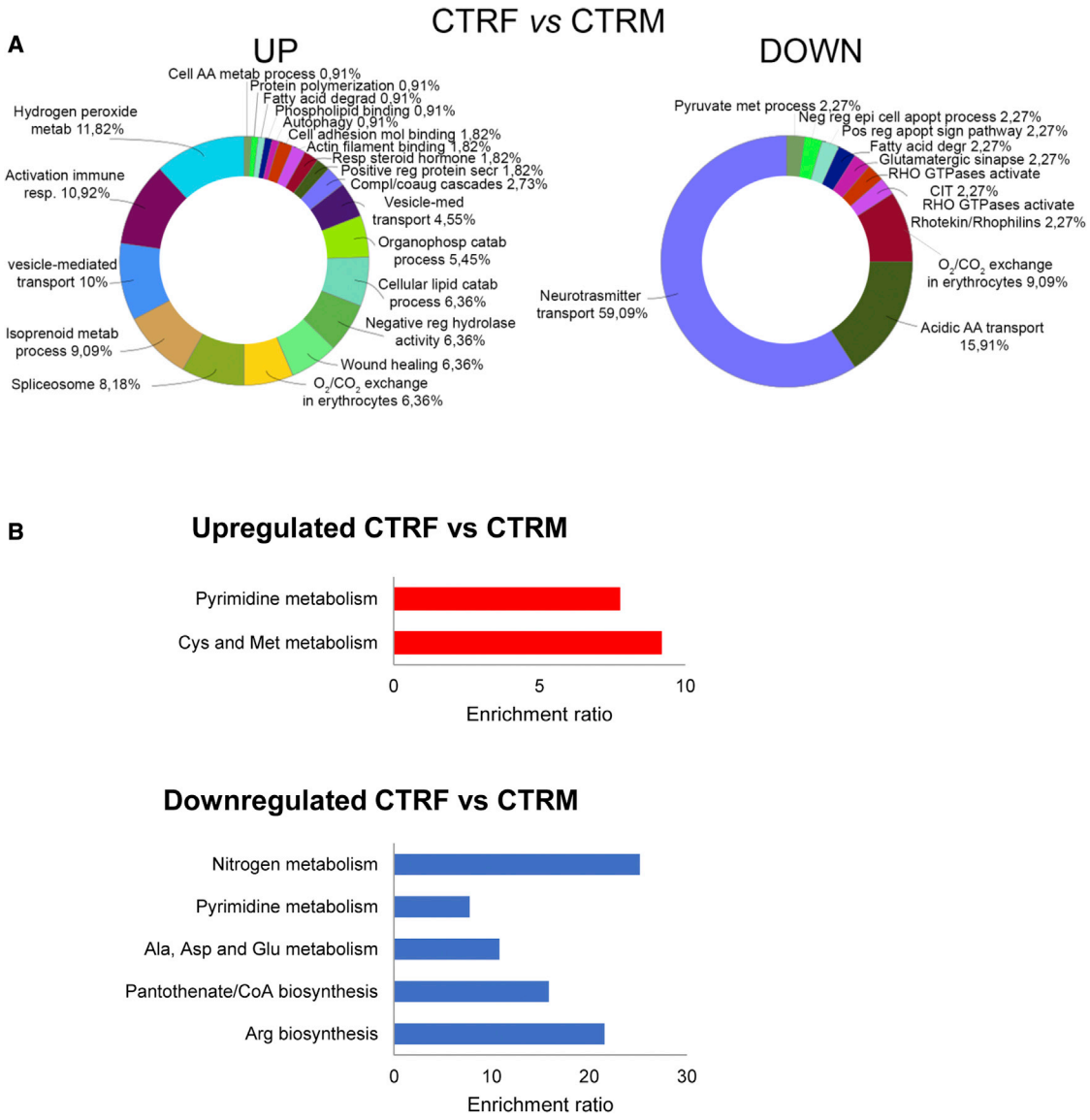

Figure 2. Proteomics and metabolomics comparison between sexes for CTR in hippocampal samples

(A) Bioinformatics analyses were carried out using ClueGo software (Cytoskape release 3.8.2) to cluster enriched annotation groups of biological processes, pathways, and networks within the set of DEPs to compare CTRF and CTRM. Functional grouping was based on Fisher's exact test ($p \leq 0.05$) and at least 3 counts.

(B) Metabolite enrichment analysis of upregulated and downregulated pathways in CTRF compared with CTRM. All upregulated metabolites were identified and analyzed using MetaboAnalyst 5.0 software. Metabolomic analysis was performed by gas chromatography-mass spectrometry (GC-MS) and liquid chromatography-MS (LC-MS) on five biological replicates for each group, each analyzed in technical duplicate.

See also Figures S2 and S3; data are reported in Tables S4, S5A, and S6.

mouse models of AD (Demarest et al., 2020). In particular, an increase in glucose-6-phosphate, whose level has been reported to increase in the mouse brain during aging (Ding et al., 2021), was found in AD samples. A similar glucose-6-phosphate increase was also observed in the serum of AD mouse models and in the AD human inferior frontotemporal gyrus (Demarest et al., 2020), indicative of alterations in the glycolytic pathway associated with AD. In keeping with these findings, we observed downregulation of lactic acid in the hippocampus, as reported previously in serum from individuals with AD (Demarest et al., 2020).

Evidence highlights differences in the levels of many metabolites between the sexes under normal conditions in serum (Krumsiek et al., 2015), but little is known about this issue in postmortem brain tissues. Accordingly, metabolomics profiles of hippocampal tissues considering sex separation were compared. All healthy male (n = 9) and female (n = 11) samples (Table S1) were well separated in the PLS-DA analysis (Figure S3A). Of the

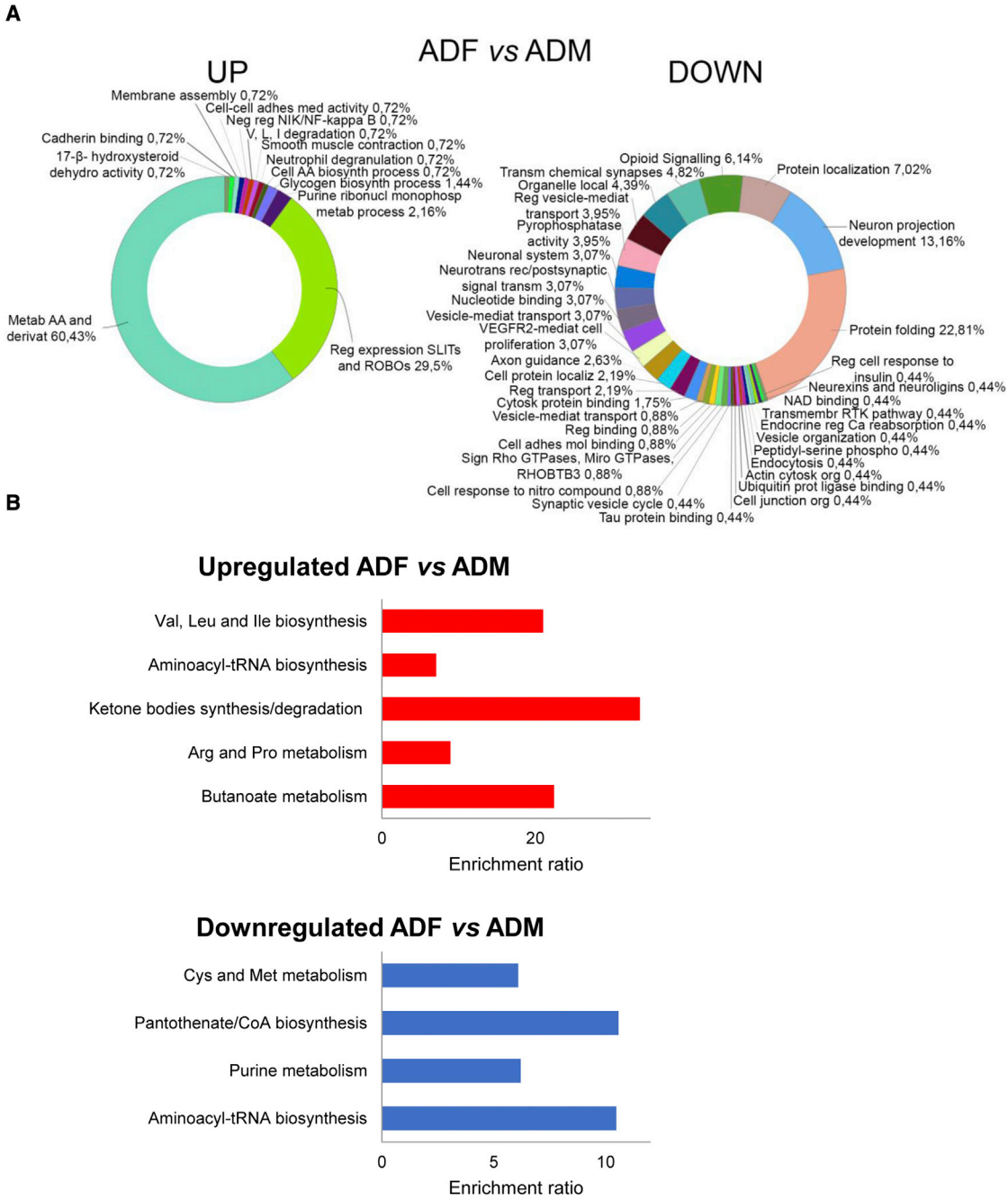

Figure 3. Proteomics and metabolomics comparison between sexes for AD in hippocampal samples

(A) Bioinformatics analyses were carried out by CLUEGO software (see legend of Figure 2) within the set of DEPs in the ADF versus ADM comparison.

(B) Metabolite enrichment analysis of upregulated and downregulated pathways in ADF compared with ADM. All differently regulated metabolites were identified and analyzed using MetaboAnalyst 5.0 software.

See also Figures S2 and S3A; data are reported in Tables S4, S5D, and S6.

126 metabolites detected, 20 were significantly different between the sexes ($p < 0.05$), half of which were upregulated and half downregulated in CTRF compared with CTRM (Table S6). Among the downregulated ones were nitrogen metabolism, Ala/Asp/Glu and Arg metabolism, and pantothenate and CoA biosynthesis, whereas Cys/Met metabolism was higher in CTRF than in CTRM, and metabolites of the pyrimidine pathway were up- and downregulated (Figure 2B).

Regarding the CTRM and ADM comparison, PLS-DA analysis shows that CTR (n = 9) and AD (n = 11) samples were

CTRF *vs* CTRM

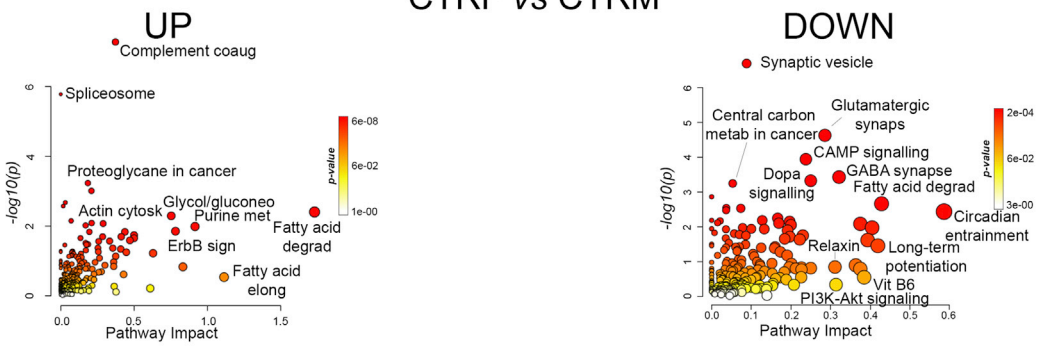

ADM *vs* CTRM

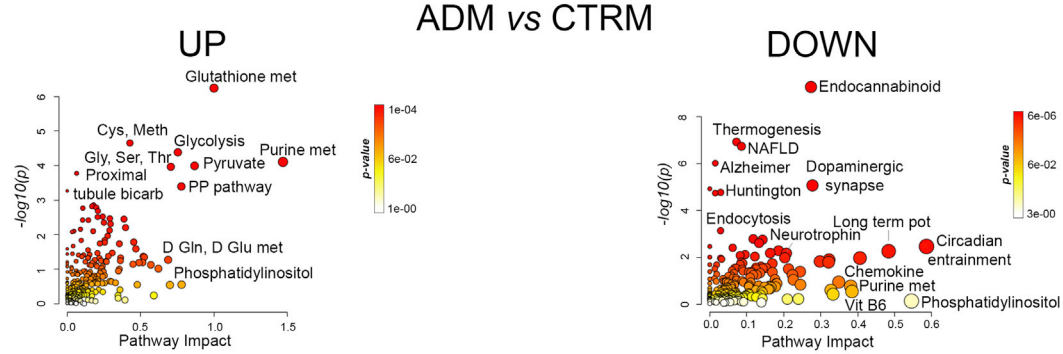

ADF *vs* CTRF

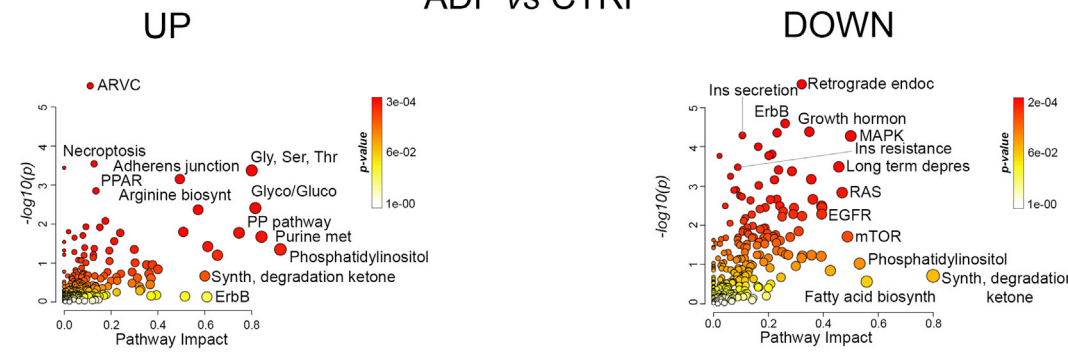

ADF *vs* ADM

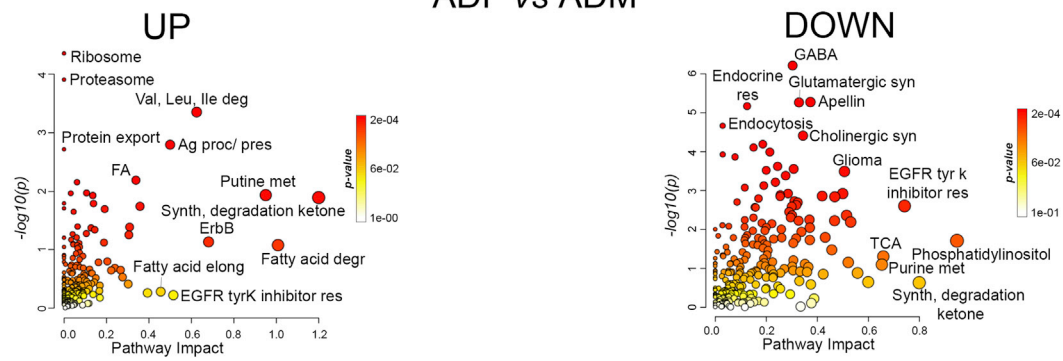

(legend on next page)

well separated among men (Figure S3A). Of the 126 metabolites detected, 25 were significantly different in CTRM versus ADM brain tissues (12 and 13 up- and downregulated, respectively) (Table S6). Set enrichment analysis revealed that the PPP and Val/Leu/Ile biosynthesis were the most up- and downregulated in ADM, respectively, whereas metabolites of the pyrimidine metabolism were up- and downregulated (Figure S3C).

Comparing female hippocampal tissues of CTRs (n = 11) versus disease condition (n = 12), the groups could be well distinguished by PLS-DA analysis (Figure S3A). Among 126 metabolites detected, 30 were significantly different in ADF brain tissues compared to CTRF, half of which were upregulated and half downregulated (Table S6). Set enrichment analysis showed that Arg biosynthesis and the PPP were upregulated in ADF, whereas Gly/Ser/Thr, Cys/Met, and Ala/Asp/Glu metabolism, along with several other pathways related to carbon metabolism, were among the most significantly downregulated ones (Figure S3D).

In accordance with the proteomics analysis, sex differences were better highlighted when comparing ADF and ADM samples (Figure 3B; Table S6). Among 126 metabolites detected, 25 were significantly different in ADF brain tissues compared with ADM, with 10 and 15 up- and downregulated, respectively. Val/Leu/Ile and Arg/Pro metabolism and butanoate and ketone body metabolism were prevalent in ADF in comparison with ADM, whereas purine metabolism as well as Cys/Met metabolism and pantothenate and CoA biosynthesis (downregulated in ADF versus CTRF; Figure S3D) were significantly downregulated in ADF (Figure 3B).

Proteomics and metabolomics data integration highlights sex differences

Integrating proteomics and metabolomics data using Metaboanalyst 5.0 software clearly suggests that, in CTRF, the processes related to energetic metabolism (TCA cycle, glycolysis, gluconeogenesis, pyruvate, and PPP) were upregulated in comparison with CTRM, together with HIF-1 signaling pathway, focal adhesion, actin cytoskeleton regulation, adherens junction, and metabolism of purine and various amino acids (especially Cys, Met, Val, Leu, and Ile) (Figure 4; Table S7). In contrast, Ala, Asp, and Glu metabolism; Arg biosynthesis; and glutamatergic synapse were prevalent in men (Figure 4; Table S7).

Some of the major pathways enriched in healthy women compared with men were also increased in ADF versus CTRF and in ADM compared with CTRM: glycolysis, PPP, Cys/Met, pyruvate and purine metabolism, and adherens junction. Other pathways higher in CTRF versus CTRM decreased in ADF versus ADM (i.e., the TCA cycle and ErbB signaling pathway) (Figure 4; Table S7). On the other hand, pathways such as Arg biosynthesis and Ala, Asp, and Glu metabolism, which were more upregulated in CTRM than in CTRF, were higher in AD independent of sex. Proteins involved in the insulin pathway and secretion presented a sex-dependent distribution in AD: they were lower in ADF than in ADM and in ADF versus CTRF but higher in ADM than in CTRM. The AD changes, in some respects, almost reverse the sex-specific proteomics and metabolomics profiles.

Ser metabolism of hippocampal brain tissues reveals sex-based differences

Given the recent association between AD progression and Ser metabolism (Piubelli et al., 2021), we focused on genes, enzymes, and metabolites of the Ser biosynthesis pathway. Transcriptomics data indicate that the *PHGDH*, *PSAT*, and *PSP* genes encoding the PP enzymes were expressed at comparable levels in the hippocampus of CTR and AD subjects (Figure S4A). Differential transcript usage (DTU) analysis by DRIMSeq did not reveal any difference in the isoform landscape of these genes in AD samples compared with CTRs (Figure S4A; Table S8A). Similar results were obtained for genes encoding SR and DAAO, the enzymes involved in D-Ser metabolism (Pollegioni and Sacchi, 2010); changes never reached a statistical significance (Figure S4A). Neither the gene coding Ser dehydratase (SDH) nor the one coding Ser hydroxymethyltransferase 2 (SHMT2; the mitochondrial isoform of the enzyme), which connects Ser to Gly, was altered in AD samples. Overall, the enzymes involved in the L- and D- Ser pathway were not regulated differently at the transcriptional level in individuals with AD and healthy CTRs, at least in the hippocampus.

In contrast, proteomics analysis of Ser metabolism highlighted significant differences in the hippocampus of individuals with AD. PSAT, PHGDH, and SR levels increased in individuals affected by AD compared with CTRs (Figure 5), whereas PSP and DAAO levels were below the detection limit of the instrumental setup. Considering sex separation, SR expression was detected in healthy men, whereas it was below detection in female subjects (Figure 5; Table S5A) and was higher in female and male individuals with AD than in CTRs (Tables S5C and S5D). The differences for PHGDH and PSAT did not reach statistical significance between sexes in healthy and AD subjects. However, PHGDH significantly increased in ADF and ADM, and PSAT showed a statistical difference in AD versus CTR in men only (Figure 5). When comparing ADF and ADM samples, no statistically significant differences were observed for PP enzymes, whereas SR expression was higher in AD-affected women. For all comparisons, no changes were observed in SHMT2 expression (Table S5). In contrast, expression of the SDH-like (SDSL) enzyme, which catalyzes threonine and Ser deamination with different K_M values (one order higher for Thr), was significantly increased in individuals with AD (Table S5D), similar to that observed for SR.

The expression levels of some of these enzymes were evaluated further by western blot analysis (Figures 5 and S4B). Only

Figure 4. Proteomics and metabolomics data integration

Integration of proteomics and metabolomics data was performed using MetaboAnalyst software R5.0 based on a Fisher's exact test ($p \leq 0.05$). Color intensity (white to red) reflects increasing statistical significance based on the p value [−log p] from the pathway enrichment analysis, and circle dimension is based on pathway impact values from the pathway topology analysis (0–1). For clarity, only the most important pathways in terms of enrichment and impact are reported; the full list is shown in Table S7.

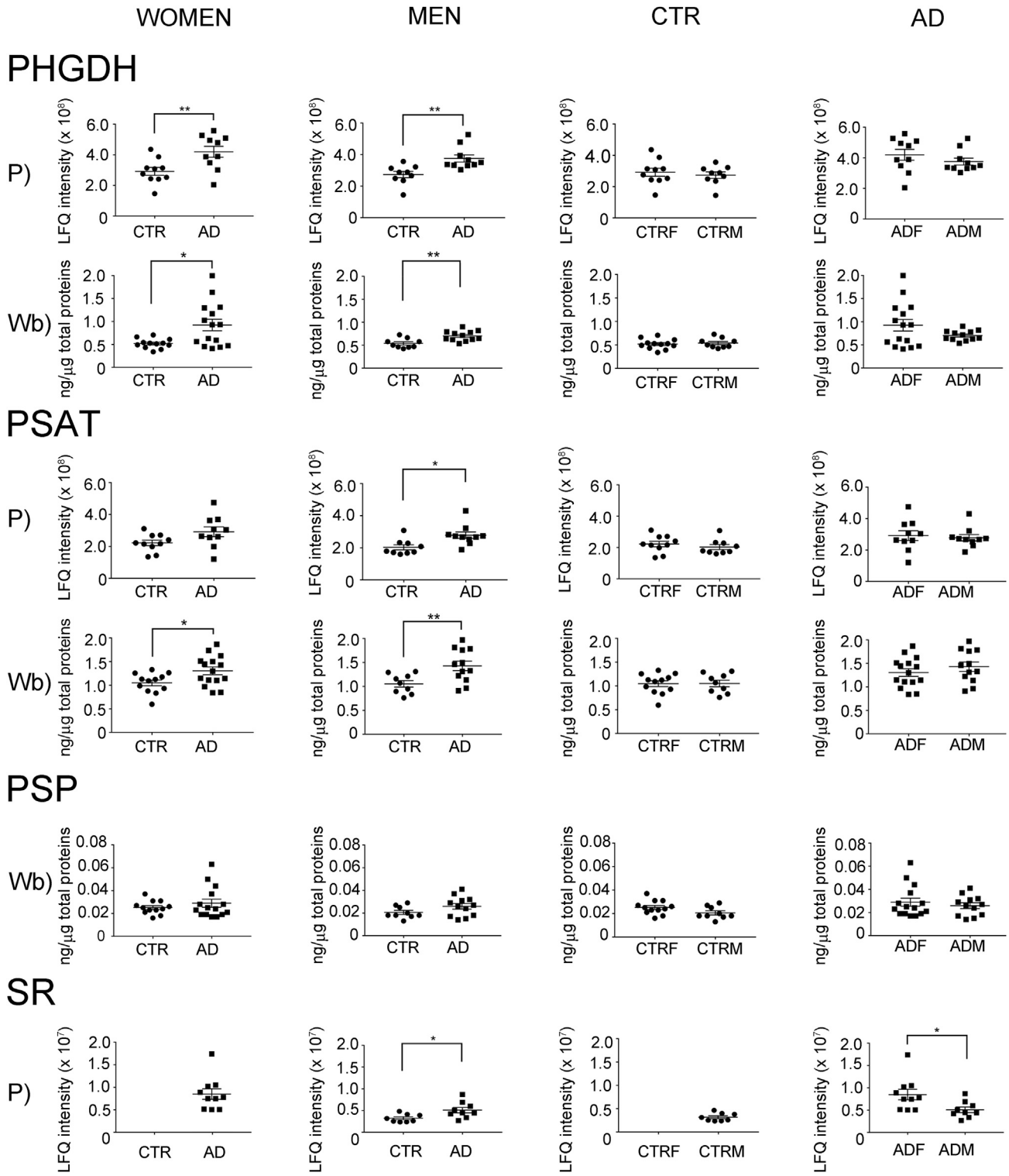

Figure 5. Comparison of the expression of PP enzymes (PHGDH, PSAT, and PSP) and SR in CTR and AD hippocampal samples

(P) indicates panels showing proteomics analysis, with the median of label-free quantification (LFQ) intensity values obtained from 5 replicates in each group, analyzed by Student's t test (*$p < 0.05$). (Wb) indicates panels showing western blot analysis, with graphs reporting single data points (dots, corresponding to single biological replicates analyzed in at least 3 technical replicates); see Figure S4B. Bars represent the means ± SEM of values obtained from 21 healthy CTRs (9 men, 12 women) and 27 individuals with AD (12 men, 15 women); *$p < 0.05$, **$p < 0.01$. Data are reported in Tables S5 and S8B.

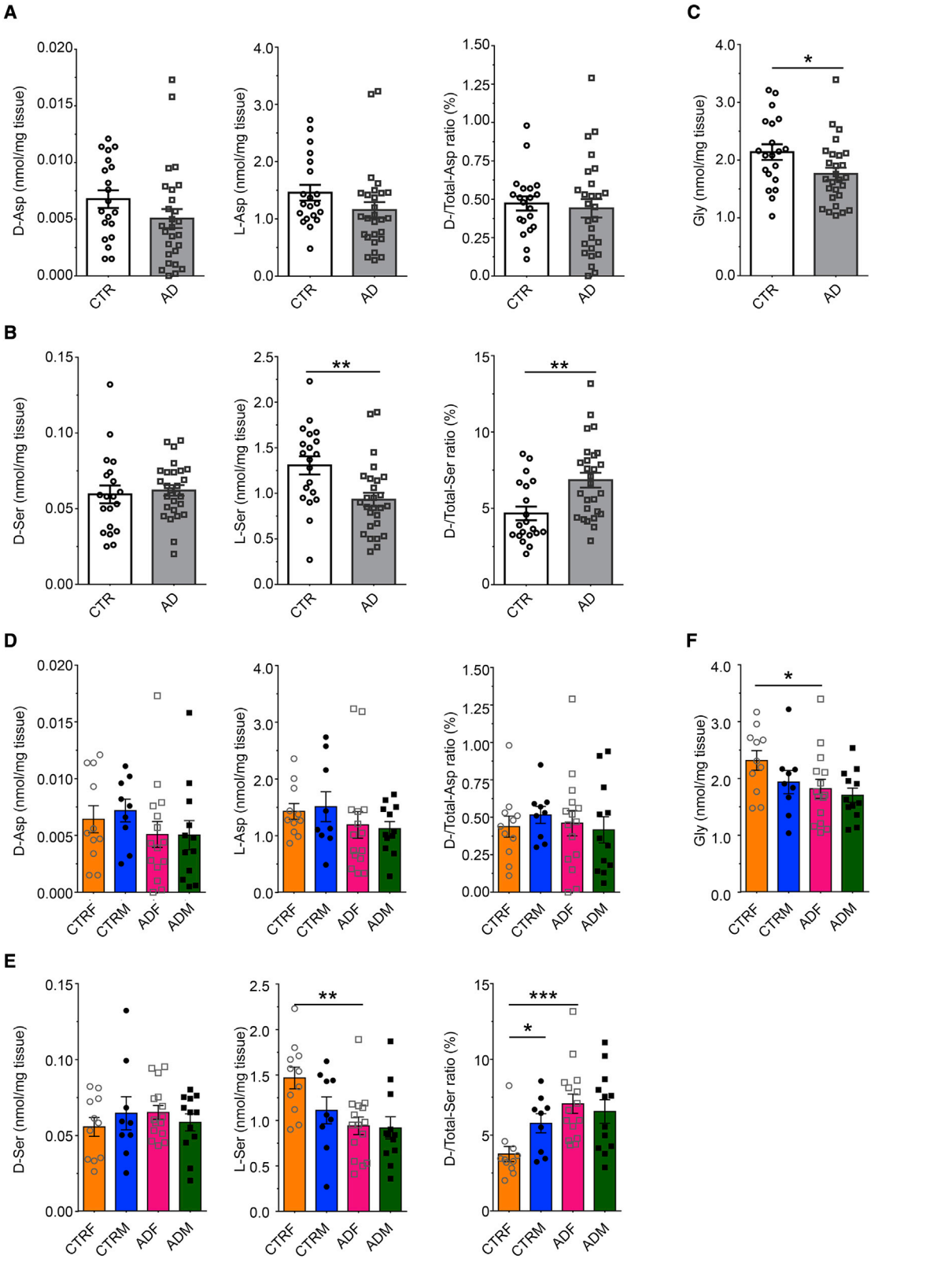

(legend on next page)

one relevant band was detected for each protein: at 57 kDa for PHGDH, at 40 kDa for PSAT, and at 30 kDa for PSP. PSP showed the lowest expression (~25- to 50-fold lower than those for PHGDH and PSAT), with no changes in protein levels between the different conditions (Table S8B). In contrast, PHGDH and PSAT levels were significantly increased in individuals affected by AD, in line with the proteomics data (Figure 5). When data were disaggregated by sex, a significant statistical increase in levels of PHGDH and PSAT was apparent for men and women with AD. Again, no differences were observed in PSP levels for male or female AD samples compared with CTRs.

At the metabolomics level, a statistically significant lower Ser level was apparent in ADF samples compared with CTRF as well as in ADF versus ADM (Table S6). To examine the contribution of L- and D- enantiomers in depth, levels of Ser and Asp enantiomers and those of Gly were determined by enantiomeric high-pressure liquid chromatography (HPLC) (Figure 6; Table S8C). A decreased L-Ser level in AD versus CTR samples was observed (−28.74%) and was coupled with an increase in D-Ser levels (+4.35%, not reaching a statistically significant threshold); a statistically significant increase for the D/total Ser ratio was observed in individuals with AD (+46.76%; Figure 6B). No significant alterations in the levels of D-Asp, L-Asp, and D/total Asp were detected (Figure 6A). A statistically significant decrease in Gly levels was determined for AD compared with CTRs (−17.70%; Figure 6C). When sex separation was considered, still no significant differences in Asp levels were found between AD and CTR samples (Figure 6D). However, sex did affect the Ser enantiomers (Figure 6E). In ADF, L-Ser levels were lower (−35.95%), in keeping with the metabolomics analysis (Table S6), resulting in a significant 2-fold increase in the D/total-Ser ratio, whereas no significant differences were found in men with AD and CTRs (Figure 6E). Gly levels decreased for ADF compared with CTRF (−21.61%, Figure 6F).

These data indicate that the Ser/Gly pathway (Figure S5) is mainly altered in women with AD.

DISCUSSION

During aging, the brain undergoes metabolic changes that primarily involve glucose metabolism, glucose transport, and insulin signaling, with consequent alterations and an imbalance in other intracellular metabolic cascades. Thus, it is crucial to compare these age-associated metabolic alterations with those occurring in AD for developing new therapeutic strategies for this age-associated, devastating dementia. A recent analysis of the literature on the whole central nervous system (Altiné-Samey et al., 2021) showed that the pathways most significantly altered in AD are Arg biosynthesis and Ala/Asp/Glu metabolism, whose metabolites were also confirmed to be significantly changed in our study (Figures 4 and S3B; Table S7).

Starting from transcriptional analyses, our study highlights a strong sex effect under normal aging and AD conditions, particularly relevant for insulin signaling and amino acid metabolism. Integration of proteomics and metabolomics data clearly shows that some pathways are enriched in AD irrespective of sex: glycolysis/gluconeogenesis, PPP, pyruvate pathway, Cys/Met, purine metabolism, adherens junctions, focal adhesion, Ala/Asp/Glu metabolism, Arg biosynthesis, and glutamatergic synapses (Figure 7A). Sex-associated differences are apparent in healthy CTRs and individuals with AD. Under healthy conditions, specific pathways are enriched in women when comparing CTRF and CTRM (glycolysis/gluconeogenesis, PPP, pyruvate pathway, Cys/Met, purine metabolism, adherens junctions, and focal adhesion), whereas Ala/Asp/Glu metabolism, Arg biosynthesis, and glutamatergic synapses are lower in CTRF versus CTRM (Figure 7).

TCA cycle, ErbB signaling, and HIF-1 pathway/insulin secretion are higher in CTRF versus CTRM. Also, they are lower in ADF versus ADM, indicating that they are completely overturned under disease conditions (Figure 7A). In particular, proteins involved in insulin growth factor (IGF) transport and uptake are increased in CTRF versus CTRM. Conversely, in ADF versus ADM, there is a decrease in proteins involved in the response to insulin stimulus and in GLP1 (glucagon-like peptide-1) regulation of insulin secretion, some of which are implicated in GABAergic synapses and circadian entrainment. Hyperinsulinemia and insulin resistance have been demonstrated to have significant effects on cognitive impairment, to play a significant role in AD, and to be prevalent among female subjects (Simsir et al., 2018). GLP1 is a 30-amino-acid incretin hormone known to act as a neuropeptide in the brain and to show neurotrophic and neuroprotective effects in the central nervous system (Xie et al., 2021) and in AD. Therefore, the decrease in GLP1 regulation of insulin secretion in ADF in comparison with ADM may contribute to the marked difference in AD incidence between sexes (Figure 7A).

Accumulating evidence is demonstrating that hyperglycemia is a potential risk factor for development of AD and that a low insulin response is associated with a higher risk for AD. Accordingly, our proteomics data show increased expression of IGF-binding protein 7 (IGFBP7), which is apparent in ADF (Table S5D). Secretion of this protein is upregulated in response to oxidative stress and linked to insulin resistance and impaired insulin signaling in AD, being a critical regulator of memory consolidation (Agbemenyah et al., 2014). Differences can be also observed regarding the expression of mitochondrial

Figure 6. Levels of Ser and Asp enantiomers and of Gly in hippocampal samples

(A–C) D- and L-Asp (A; left and center, respectively), D- and L-Ser (B; left and center, respectively), and Gly (C) levels and ratio between D/total amino acid content (A and B, right, for Asp and Ser, respectively) detected in the hippocampus of individuals with AD compared with healthy subjects (CTR); see Table S8C. Values from metabolomic analysis are reported in Table S6.

(D–F) Sex variations of D- and L-Asp (D, left and center panels, respectively), D- and L-Ser (E, left and center panels, respectively), and Gly (F) and ratio between D/total amino acid content (D and E, right panel for Asp and Ser, respectively) of individuals with AD compared with healthy CTRs. Graphs report single data points (corresponding to single biological replicates analyzed in 3–6 technical replicates) as well as mean values ± SEM. *$p < 0.05$, **$p < 0.01$, ***$p < 0.0001$ (Mann-Whitney unpaired test).

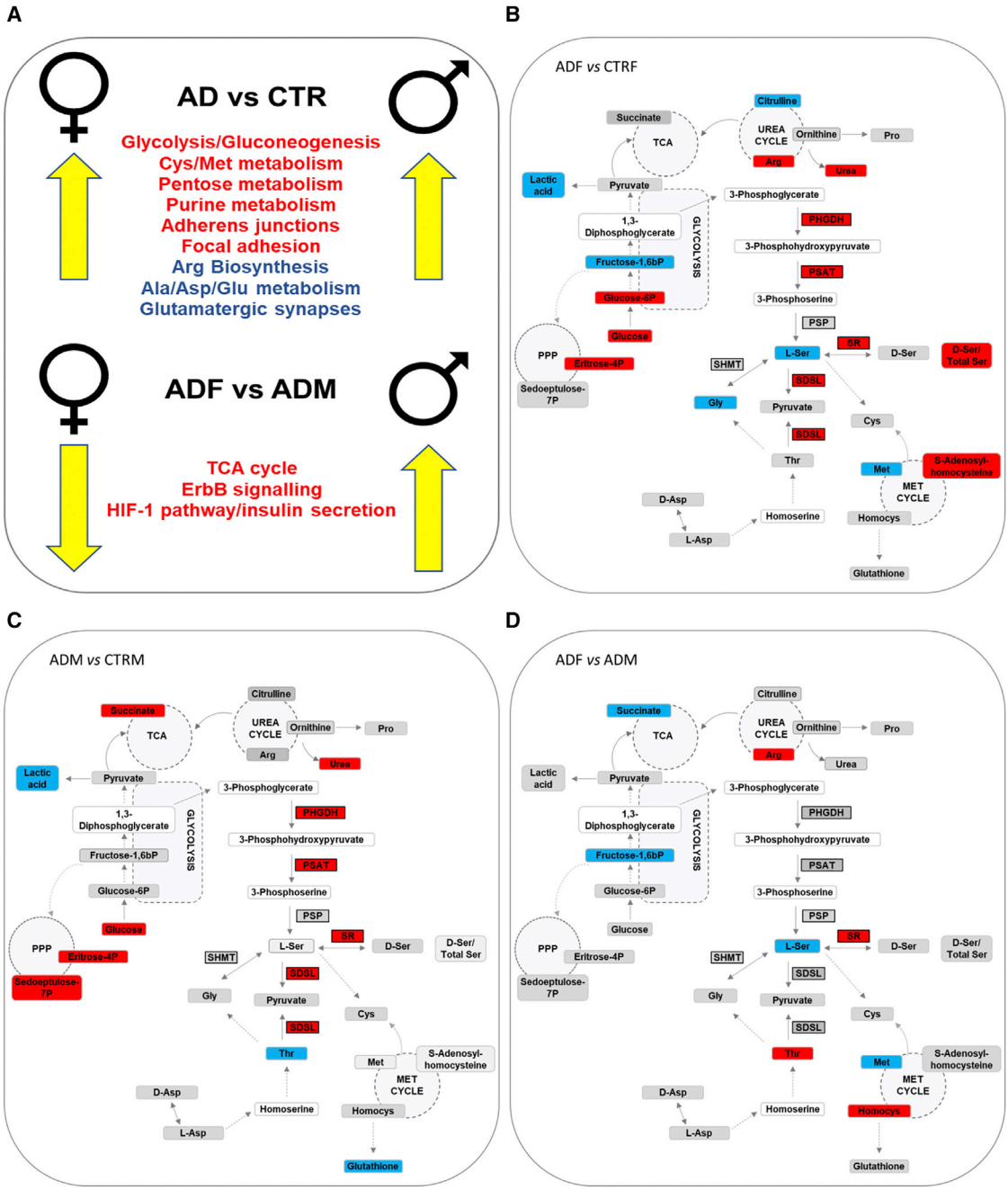

Figure 7. Comparison between sexes during healthy aging and AD onset

(A) Graphical representation of the enrichment pathways of healthy men and women and those with AD. Integration between proteomics and metabolomics data was performed using MetaboAnalyst software R5.0 based on a Fisher's exact test ($p \leq 0.05$). The top panel reports pathways higher in women with AD (ADF versus CTRF) and men with AD (ADM versus CTRM). The bottom panel reports pathways higher in ADM and lower in ADF when comparing ADF and ADM. In both panels, the pathways higher in healthy women (CTRF versus CTRM) are indicated in red, and shown in blue are those higher in men (CTRF versus CTRM). (B–D) Schematic of enzymes and metabolic pathways when comparing ADF and CTRF (B), ADM and CTRM (C), and ADF and ADM (D). Red and blue indicate upregulation and downregulation, respectively.

pyruvate carrier 1 (MPC1), which shows a statistically significant reduction in ADM versus CTRM (Table S5D; Figure S4C), resembling that reported previously in *Drosophila* (Yamazaki et al., 2014). MPC1 is thought to play a central role in glucose-stimulated insulin secretion, systemic glucose homeostasis in β cells, and in the insulin-resistant state (McCommis et al., 2016). These data indicate how different pathophysiological mechanisms are active in men and women (Figure 7A).

The metabolism of amino acids is the most altered pathway. Human postmortem brain tissue research has shown that disturbances in Arg metabolism accompany AD and contribute to its pathogenesis. The increase in Arg/Pro metabolism in AD, confirmed also by our results (Figure 7), is more apparent in ADF than ADM (Figure 3B) and correlates with the higher rate of tau aggregation and amyloid burden and deposition that have been reported in women relative to men (Wang et al., 2003; Smith et al., 2020). The Arg/Pro metabolism, via its related metabolites (Cohen and Nadler, 1997; Kotagale et al., 2020), may also contribute to the dysfunction of NMDAR signaling in AD (Zhang et al., 2016; Liu et al., 2019). NMDAR signaling is specifically related to the metabolism of the coagonist D-Ser and closely linked to energetic metabolism. A recent study reported that extracellular levels of L- and D-Ser were reduced at an early stage of AD, before β-amyloid plaque was deposited in the hippocampus of a mouse model that displays lower glycolytic flux in hippocampal astrocytes (Le Douce et al., 2020). The glycolytic flux may control brain L-Ser synthesis (Figure S5); phosphoglycerate kinase (PGK) and phosphoglycerate mutase (PGM1) are mainly responsible for the relatively high levels of cellular L-Ser (0.18–0.55 mM) (Jin et al., 2020) because the K_M of human PHGDH for 3PG (0.36 mM) is larger than its cellular level (Murtas et al., 2021). Although human PHGDH activity is not affected by L-Ser (Murtas et al., 2021), the pyruvate kinase M2 isoform (PKM2, mainly expressed in tumor cells and in astrocytes) is activated by L-Ser binding (Chaneton et al., 2012), supporting glycolysis and lactate production. Conversely, at low L-Ser levels, the glycolytic flux to lactate is transiently reduced, favoring accumulation (doubling) of 3PG, which can be rerouted to produce L-Ser (Ye et al., 2012); a bidirectional control between PP and glycolysis is active (Figure S5). Glucose controls acetylation of K58 in PHGDH; a decrease in glucose level, by decreasing acetylation, pushes PHGDH degradation through RNF5 E3 ubiquitin ligase, yielding a decrease in Ser and Gly levels, reactive oxygen species increase, and cell growth inhibition (Wang et al., 2020). PHGDH and Ser metabolism are directly regulated by NAD^+/NADH availability in the cytosol (a ratio strictly linked to glycolysis), and Ser feeds NADH to mitochondria when respiration is impaired (Yang et al., 2020). Our results show an increase in PHGDH, PSAT, and SR levels in AD hippocampal samples (Figures 5 and 7B), in good agreement with the increase determined in brains of individuals affected by AD (Yan et al., 2020; Chen et al., 2022), as a mechanism to increase NMDAR activity by providing more D-Ser. The effect of sex on Ser levels might affect long-term potentiation (LTP) differently. (1) In healthy men, the increase in D-Ser/total Ser ratio should represent a way to counteract age-related cognitive decline mainly related to learning and memory (Balu and Coyle, 2015), in keeping with the study by Yamazaki et al. (2014) in *Drosophila*, reporting that, during aging in men, the reduced pyruvate levels are paralleled by increased D-Ser levels (as reported for the human samples in Figures 6E and 7B), resulting in decreased age-related memory impairment. (2) Analogously, the higher D-Ser/total Ser ratio levels should make it possible to increase LTP in women during AD onset, reaching values resembling those determined in CTRM (Figure 6). This represents a specific attempt to rescue NMDAR hypofunction by overproducing D-Ser from SR and the PP, in perfect agreement with the observed increase in blood D-Ser levels during AD progression (Piubelli et al., 2021). Of course, NMDAR stimulation by D-Ser is a two-edged sword; increasing D-Ser in the early phases of AD might be beneficial because it can inhibit apoptosis (Esposito et al., 2012), but excessive D-Ser release induced by β-amyloid (Aβ) aggregates (Wu et al., 2004) or PHGDH increase (Chen et al., 2022) contributes to neuronal death through excitotoxicity.

Our data, together with previous reports, suggest that NMDAR activation might be regulated in two different ways in individuals with AD: by increasing the Arg/Pro metabolism in both sexes, which could contribute to NMDAR overactivation by stimulating Ca^{2+} entry (Henzi et al., 1992), and by increasing the level of the coagonist D-Ser in women only. This proposal suggests that a further mechanism contributes to those underlying the known sex differences in Glu systems in AD (Wickens et al., 2018) that have been ascribed to the interaction of the glutamatergic system with sex hormones: "As women age, their estrogen levels decline and this decline in estrogen may increase vulnerability" to AD (Pike, 2017). Tau pathology further contributes to reducing estrogen activity in the AD brain by sequestering estrogen receptor α in the cytoplasm (Wang et al., 2016). Whether this effect is more deleterious in women than in men should be investigated, as should the effects of androgens, whose levels decline in aged men and women (Raber, 2004), and the altered estrogen/androgen balance.

Limitations of this study

This work is hindered by a limited number of analyzed samples (21 CTR and 27 AD samples, selected for their quality) and by their European origin only (Table S1).

STAR★METHODS

Detailed methods are provided in the online version of this paper and include the following:

- KEY RESOURCES TABLE
- RESOURCE AVAILABILITY
  - Lead contact
  - Materials availability
  - Data and code availability
- EXPERIMENTAL MODEL AND SUBJECT DETAILS
  - Patient cohorts and brain samples
- METHOD DETAILS
  - RNA extraction, libraries, and sequencing
  - Preprocessing and analysis of RNA-seq data
  - Mass-spectrometry-based proteomics analysis
  - Metabolites extraction
  - Metabolic profiling
  - Western blot analysis
  - Enantiomeric HPLC analysis
- QUANTIFICATION AND STATISTICAL ANALYSIS
  - RNA-seq data analysis
  - Label-free proteomics
  - Metabolic profiling
  - Western blot analysis
  - Enantiomeric HPLC analysis

SUPPLEMENTAL INFORMATION

Supplemental information can be found online at https://doi.org/10.1016/j.celrep.2022.111271.

ACKNOWLEDGMENTS

This paper is dedicated to the memory of N.C. This research was funded by a grant from Ministero Università e Ricerca Scientifica PRIN 2017 (2017H4J3AS) to L.P. (as coordinator) and to G.B., P.C., and N.C. (as unit responsible). We also acknowledge financial support from the Italian Ministry of University and Research (MiUR) through grant "Dipartimenti di Eccellenza 2017" to the University of Milano-Bicocca, Department of Biotechnology and Biosciences. We thank UNITECH OMICS of the University of Milano for proteomics data acquisition and Dr. Tamara Canu from the Preclinical Imaging Facility (CIS), Ospedale San Raffaele, Milan. We also thank Dr. Armando Negri, Viviana Triaca, and Marco Vanoni for useful comments.

AUTHOR CONTRIBUTIONS

L.P., G.T., P.C., and N.C. designed the project and conceptualized the approach. G.M. performed western blot analyses. V.R. and Z.M. performed HPLC analyses. S.S. set up analytical methods and prepared the STAR Methods section. E.M. designed and performed the proteomics analysis. S.N. performed sample preparation and proteomics analysis. F.I. and A.M.R. extracted RNA samples. D.L. performed transcriptome analysis. All authors performed data curation and wrote the original draft. B.B. and F.T. analyzed metabolomics data. E.M., G.M., V.R., F.T., B.B., and N.C. prepared illustrations. All authors have read and agreed to the published version of the manuscript.

DECLARATION OF INTERESTS

The authors declare no competing interests.

Received: August 28, 2021
Revised: July 1, 2022
Accepted: August 5, 2022
Published: September 6, 2022

REFERENCES

Agbemenyah, H.Y., Agis-Balboa, R.C., Burkhardt, S., Delalle, I., and Fischer, A. (2014). Insulin growth factor binding protein 7 is a novel target to treat dementia. Neurobiol. Dis. *62*, 135–143. https://doi.org/10.1016/j.nbd.2013.09.011.

Altiné-Samey, R., Antier, D., Mavel, S., Dufour-Rainfray, D., Balageas, A.C., Beaufils, E., Emond, P., Foucault-Fruchard, L., and Chalon, S. (2021). The contributions of metabolomics in the discovery of new therapeutic targets in Alzheimer's disease. Fundam. Clin. Pharmacol. *35*, 582–594. https://doi.org/10.1111/fcp.12654.

Altmann, A., Tian, L., Henderson, V.W., and Greicius, M.D.; Alzheimer's Disease Neuroimaging Initiative Investigators (2014). Alzheimer's disease neuroimaging initiative investigators. Sex modifies the APOE-related risk of developing Alzheimer disease. Ann. Neurol. *75*, 563–573. https://doi.org/10.1002/ana.24135.

Armada-Moreira, A., Gomes, J.I., Pina, C.C., Savchak, O.K., Gonçalves-Ribeiro, J., Rei, N., Pinto, S., Morais, T.P., Martins, R.S., Ribeiro, F.F., et al. (2020). Going the extra (synaptic) mile: excitotoxicity as the road toward neurodegenerative diseases. Front. Cell. Neurosci. *14*, 90. https://doi.org/10.3389/fncel.2020.00090.

Arnold, M., Nho, K., Kueider-Paisley, A., Massaro, T., Huynh, K., Brauner, B., MahmoudianDehkordi, S., Louie, G., Moseley, M.A., Thompson, J.W., et al. (2020). Sex and APOE ε4 genotype modify the Alzheimer's disease serum metabolome. Nat. Commun. *11*, 1148. https://doi.org/10.1038/s41467-020-14959-w.

Baloni, P., Funk, C.C., Yan, J., Yurkovich, J.T., Kueider-Paisley, A., Nho, K., Heinken, A., Jia, W., Mahmoudiandehkordi, S., Louie, G., et al. (2020). Metabolic network analysis reveals altered bile acid synthesis and metabolism in Alzheimer's disease. Cell Rep. Med. *1*, 100138. https://doi.org/10.1016/j.xcrm.2020.100138.

Balu, D.T., and Coyle, J.T. (2015). The NMDA receptor 'glycine modulatory site' in schizophrenia: D-serine, glycine, and beyond. Curr. Opin. Pharmacol. *20*, 109–115. https://doi.org/10.1016/j.coph.2014.12.004.

Bindea, G., Mlecnik, B., Hackl, H., Charoentong, P., Tosolini, M., Kirilovsky, A., Fridman, W.H., Pagès, F., Trajanoski, Z., and Galon, J. (2009). ClueGO: a Cytoscape plug-in to decipher functionally grouped gene ontology and pathway annotation networks. Bioinformatics *25*, 1091–1093. https://doi.org/10.1093/bioinformatics/btp101.

Butterfield, D.A., and Halliwell, B. (2019). Oxidative stress, dysfunctional glucose metabolism and Alzheimer disease. Nat. Rev. Neurosci. *20*, 148–160. https://doi.org/10.1038/s41583-019-0132-6.

Chaneton, B., Hillmann, P., Zheng, L., Martin, A.C.L., Maddocks, O.D.K., Chokkathukalam, A., Coyle, J.E., Jankevics, A., Holding, F.P., Vousden, K.H., et al. (2012). Serine is a natural ligand and allosteric activator of pyruvate kinase M2. Nature *491*, 458–462. https://doi.org/10.1038/nature11540.

Chen, X., Calandrelli, R., Girardini, J., Yan, Z., Tan, Z., Xu, X., Hiniker, A., and Zhong, S. (2022). Sequential increase of PHGDH expression with Alzheimer's pathology and symptoms. Preprint at bioRxiv. https://doi.org/10.1101/2022.02.15.480384.

Chong, J., Wishart, D.S., and Xia, J. (2019). Using MetaboAnalyst 4.0 for comprehensive and integrative metabolomics data analysis. Curr. Protoc. Bioinformatics *68*, e86. https://doi.org/10.1002/cpbi.86.

Cohen, S.M., and Nadler, J.V. (1997). Proline-induced potentiation of glutamate transmission. Brain Res. *761*, 271–282. https://doi.org/10.1016/s0006-8993(97)00352-1.

Cortes-Canteli, M., Mattei, L., Richards, A.T., Norris, E.H., and Strickland, S. (2015). Fibrin deposited in the Alzheimer's disease brain promotes neuronal degeneration. Neurobiol. Aging *36*, 608–617. https://doi.org/10.1016/j.neurobiolaging.2014.10.030.

Crist, A.M., Hinkle, K.M., Wang, X., Moloney, C.M., Matchett, B.J., Labuzan, S.A., Frankenhauser, I., Azu, N.O., Liesinger, A.M., Lesser, E.R., et al. (2021). Transcriptomic analysis to identify genes associated with selective hippocampal vulnerability in Alzheimer's disease. Nat. Commun. *12*, 2311. https://doi.org/10.1038/s41467-021-22399-3.

Daulatzai, M.A. (2017). Cerebral hypoperfusion and glucose hypometabolism: key pathophysiological modulators promote neurodegeneration, cognitive impairment, and Alzheimer's disease. J. Neurosci. Res. *95*, 943–972. https://doi.org/10.1002/jnr.23777.

Demarest, T.G., Varma, V.R., Estrada, D., Babbar, M., Basu, S., Mahajan, U.V., Moaddel, R., Croteau, D.L., Thambisetty, M., Mattson, M.P., and Bohr, V.A. (2020). Biological sex and DNA repair deficiency drive Alzheimer's disease via systemic metabolic remodeling and brain mitochondrial dysfunction. Acta Neuropathol. *140*, 25–47. https://doi.org/10.1007/s00401-020-02152-8.

Ding, J., Ji, J., Rabow, Z., Shen, T., Folz, J., Brydges, C.R., Fan, S., Lu, X., Mehta, S., Showalter, M.R., et al. (2021). A metabolome atlas of the aging mouse brain. Nat. Commun. *12*, 6021. https://doi.org/10.1038/s41467-021-26310-y.

Dobin, A., and Gingeras, T.R. (2015). Mapping RNA-seq reads with STAR. Curr. Protoc. Bioinformatics *51*, 11.14.1–11.14.19. https://doi.org/10.1002/0471250953.bi1114s51.

Esposito, S., Pristerà, A., Maresca, G., Cavallaro, S., Felsani, A., Florenzano, F., Manni, L., Ciotti, M.T., Pollegioni, L., Borsello, T., and Canu, N. (2012). Contribution of serine racemase/D-serine pathway to neuronal apoptosis. Aging Cell *11*, 588–598. https://doi.org/10.1111/j.1474-9726.2012.00822.x.

Fan, J., Ye, J., Kamphorst, J.J., Shlomi, T., Thompson, C.B., and Rabinowitz, J.D. (2014). Quantitative flux analysis reveals folate-dependent NADPH production. Nature *510*, 298–302. https://doi.org/10.1038/nature13236.

Flannery, P.J., and Trushina, E. (2019). Mitochondrial dynamics and transport in Alzheimer's disease. Mol. Cell. Neurosci. *98*, 109–120. https://doi.org/10.1016/j.mcn.2019.06.009.

Galli, A., Maffioli, E., Sogne, E., Moretti, S., Di Cairano, E.S., Negri, A., Nonnis, S., Norata, G.D., Bonacina, F., Borghi, F., et al. (2018). Cluster-assembled zirconia substrates promote long-term differentiation and functioning of human islets of Langerhans. Sci. Rep. *8*, 17472. https://doi.org/10.1038/s41598-018-35958-4.

Gamache, J., Yun, Y., and Chiba-Falek, O. (2020). Sex-dependent effect of APOE on Alzheimer's disease and other age-related neurodegenerative disorders. Dis. Model. Mech. *13*, dmm045211. https://doi.org/10.1242/dmm.045211.

Gamba, P., Giannelli, S., Staurenghi, E., Testa, G., Sottero, B., Biasi, F., Poli, G., and Leonarduzzi, G. (2021). The controversial role of 24-S-hydroxycholesterol in Alzheimer's disease. Antioxidants *10*, 740. https://doi.org/10.3390/antiox10050740.

Griffin, J.W.D., and Bradshaw, P.C. (2017). Amino acid catabolism in Alzheimer's disease brain: friend or foe? Oxid. Med. Cell. Longev. *2017*, 5472792. https://doi.org/10.1155/2017/5472792.

Henzi, V., Reichling, D.B., Helm, S.W., and MacDermott, A.B. (1992). L-Proline activates glutamate and glycine receptors in cultured rat dorsal horn neurons. Mol. Pharmacol. *41*, 793–801.

Huang, D.W., Sherman, B.T., and Lempicki, R.A. (2009). Systematic and integrative analysis of large gene lists using DAVID bioinformatics resources. Nat. Protoc. *4*, 44–57. https://doi.org/10.1038/nprot.2008.211.

Hunt, J.B., Jr., Nash, K.R., Placides, D., Moran, P., Selenica, M.L.B., Abuqalbeen, F., Ratnasamy, K., Slouha, N., Rodriguez-Ospina, S., Savlia, M., et al. (2015). Sustained arginase 1 expression modulates pathological tau deposits in a mouse model of tauopathy. J. Neurosci. *35*, 14842–14860. https://doi.org/10.1523/JNEUROSCI.3959-14.2015.

Jin, C., Zhu, X., Wu, H., Wang, Y., and Hu, X. (2020). Perturbation of phosphoglycerate kinase 1 (PGK1) only marginally affects glycolysis in cancer cells. J. Biol. Chem. *295*, 6425–6446. https://doi.org/10.1074/jbc.RA119.012312.

Johnson, E.C.B., Dammer, E.B., Duong, D.M., Ping, L., Zhou, M., Yin, L., Higginbotham, L.A., Guajardo, A., White, B., Troncoso, J.C., et al. (2020). Large-scale proteomic analysis of Alzheimer's disease brain and cerebrospinal fluid reveals early changes in energy metabolism associated with microglia and astrocyte activation. Nat. Med. *26*, 769–780. https://doi.org/10.1038/s41591-020-0815-6.

Kamburov, A., Wierling, C., Lehrach, H., and Herwig, R. (2009). ConsensusPathDB-a database for integrating human functional interaction networks. Nucleic Acids Res. *37*, D623–D628. https://doi.org/10.1093/nar/gkn698.

Kapogiannis, D., and Mattson, M.P. (2011). Disrupted energy metabolism and neuronal circuit dysfunction in cognitive impairment and Alzheimer's disease. Lancet Neurol. *10*, 187–198. https://doi.org/10.1016/S1474-4422(10)70277-5.

Kipanyula, M.J., Kimaro, W.H., and Seke Etet, P.F. (2016). The emerging roles of the calcineurin-nuclear factor of activated T-lymphocytes pathway in nervous system functions and diseases. J. Aging Res. *2016*, 5081021. https://doi.org/10.1155/2016/5081021.

Kotagale, N., Deshmukh, R., Dixit, M., Fating, R., Umekar, M., and Taksande, B. (2020). Agmatine ameliorates manifestation of depression-like behavior and hippocampal neuroinflammation in mouse model of Alzheimer's disease. Brain Res. Bull. *160*, 56–64. https://doi.org/10.1016/j.brainresbull.2020.04.013.

Krumsiek, J., Mittelstrass, K., Do, K.T., Stückler, F., Ried, J., Adamski, J., Peters, A., Illig, T., Kronenberg, F., Friedrich, N., et al. (2015). Sex-specific pathway differences in the human serum metabolome. Metabolomics *11*, 1815–1833. https://doi.org/10.1007/s11306-015-0829-0.

Le Douce, J., Maugard, M., Veran, J., Matos, M., Jégo, P., Vigneron, P.A., Faivre, E., Toussay, X., Vandenberghe, M., Balbastre, Y., et al. (2020). Impairment of glycolysis-derived L-serine production in astrocytes contributes to cognitive deficits in Alzheimer's disease. Cell Metab. *31*, 503–517.e8. https://doi.org/10.1016/j.cmet.2020.02.004.

Liao, Y., Smyth, G.K., and Shi, W. (2014). featureCounts: an efficient general-purpose program for assigning sequence reads to genomic features. Bioinformatics *30*, 923–930. https://doi.org/10.1093/bioinformatics/btt656.

Liu, J., Chang, L., Song, Y., Li, H., and Wu, Y. (2019). The role of NMDA receptors in Alzheimer's disease. Front. Neurosci. *13*, 43. https://doi.org/10.3389/fnins.2019.00043.

Love, M.I., Huber, W., and Anders, S. (2014). Moderated estimation of fold change and dispersion for RNA-seq data with DESeq2. Genome Biol. *15*, 550. https://doi.org/10.1186/s13059-014-0550-8.

Love, M. (2022). R Package Version 1.24.0.

Ma, C., Hunt, J.B., Selenica, M.L.B., Sanneh, A., Sandusky-Beltran, L.A., Watler, M., Daas, R., Kovalenko, A., Liang, H., Placides, D., et al. (2021). Arginase 1 insufficiency precipitates amyloid-β deposition and hastens behavioral impairment in a mouse model of amyloidosis. Front. Immunol. *11*, 582998. https://doi.org/10.3389/fimmu.2020.582998.

Maugard, M., Vigneron, P.A., Bolaños, J.P., and Bonvento, G. (2021). L-Serine links metabolism with neurotransmission. Prog. Neurobiol. *197*, 101896. https://doi.org/10.1016/j.pneurobio.2020.101896.

Mathys, H., Davila-Velderrain, J., Peng, Z., Gao, F., Mohammadi, S., Young, J.Z., Menon, M., He, L., Abdurrob, F., Jiang, X., et al. (2019). Single-cell transcriptomic analysis of Alzheimer's disease. Nature *570*, 332–337. https://doi.org/10.1038/s41586-019-1195-2.

McCommis, K.S., Hodges, W.T., Bricker, D.K., Wisidagama, D.R., Compan, V., Remedi, M.S., Thummel, C.S., and Finck, B.N. (2016). An ancestral role for the mitochondrial pyruvate carrier in glucose-stimulated insulin secretion. Mol. Metab. *5*, 602–614. https://doi.org/10.1016/j.molmet.2016.06.016.

Mi, H., Muruganujan, A., and Thomas, P.D. (2013). PANTHER in 2013: modeling the evolution of gene function, and other gene attributes, in the context of phylogenetic trees. Nucleic Acids Res. *41*, D377–D386. https://doi.org/10.1093/nar/gks1118.

Murtas, G., Marcone, G.L., Sacchi, S., and Pollegioni, L. (2020). L-serine synthesis via the phosphorylated pathway in humans. Cell. Mol. Life Sci. *77*, 5131–5148. https://doi.org/10.1007/s00018-020-03574-z.

Murtas, G., Marcone, G.L., Peracchi, A., Zangelmi, E., and Pollegioni, L. (2021). Biochemical and biophysical characterization of recombinant human 3-phosphoglycerate dehydrogenase. Int. J. Mol. Sci. *22*, 4231. https://doi.org/10.3390/ijms22084231.

Neame, S., Safory, H., Radzishevsky, I., Touitou, A., Marchesani, F., Marchetti, M., Kellner, S., Berlin, S., Foltyn, V.N., Engelender, S., et al. (2019). The NMDA receptor activation by D-serine and glycine is controlled by an astrocytic PHGDH-dependent serine shuttle. Proc. Natl. Acad. Sci. USA *116*, 20736–20742. https://doi.org/10.1073/pnas.1909458116.

Neff, R.A., Wang, M., Vatansever, S., Guo, L., Ming, C., Wang, Q., Wang, E., Horgusluoglu-Moloch, E., Song, W.M., Li, A., et al. (2021). Molecular subtyping of Alzheimer's disease using RNA sequencing data reveals novel mechanisms and targets. Sci. Adv. *7*, eabb5398. https://doi.org/10.1126/sciadv.abb5398.

Nonnis, S., Maffioli, E., Zanotti, L., Santagata, F., Negri, A., Viola, A., Elliman, S., and Tedeschi, G. (2016). Effect of fetal bovine serum in culture media on MS analysis of mesenchymal stromal cells secretome. EuPA Open Proteom. *10*, 28–30. https://doi.org/10.1016/j.euprot.2016.01.005.

Nowicka, M., and Robinson, M.D. (2016). DRIMSeq: a dirichlet-multinomial framework for multivariate count outcomes in genomics. F1000Research *5*, 1356. https://doi.org/10.12688/f1000research.8900.2.

Oldendorf, W.H. (1971). Brain uptake of radiolabeled amino acids, amines, and hexoses after arterial injection. Am. J. Physiol. *221*, 1629–1639. https://doi.org/10.1152/ajplegacy.1971.221.6.1629.

Paglia, G., Stocchero, M., Cacciatore, S., Lai, S., Angel, P., Alam, M.T., Keller, M., Ralser, M., and Astarita, G. (2016). Unbiased metabolomic investigation of Alzheimer's disease brain points to dysregulation of mitochondrial aspartate metabolism. J. Proteome Res. *15*, 608–618. https://doi.org/10.1021/acs.jproteome.5b01020.

Papouin, T., Ladépêche, L., Ruel, J., Sacchi, S., Labasque, M., Hanini, M., Groc, L., Pollegioni, L., Mothet, J.P., and Oliet, S.H.R. (2012). Synaptic and

extrasynaptic NMDA receptors are gated by different endogenous coagonists. Cell *150*, 633–646. https://doi.org/10.1016/j.cell.2012.06.029.

Patro, R., Duggal, G., Love, M.I., Irizarry, R.A., and Kingsford, C. (2017). Salmon provides fast and bias-aware quantification of transcript expression. Nat. Methods *14*, 417–419. https://doi.org/10.1038/nmeth.4197.

Paula-Lima, A.C., Brito-Moreira, J., and Ferreira, S.T. (2013). Deregulation of excitatory neurotransmission underlying synapse failure in Alzheimer's disease. J. Neurochem. *126*, 191–202. https://doi.org/10.1111/jnc.12304.

Pike, C.J. (2017). Sex and the development of Alzheimer's disease. J. Neurosci. Res. *95*, 671–680. https://doi.org/10.1002/jnr.23827.

Piubelli, L., Pollegioni, L., Rabattoni, V., Mauri, M., Princiotta Cariddi, L., Versino, M., and Sacchi, S. (2021). Serum D-serine levels are altered in early phases of Alzheimer's disease: towards a precocious biomarker. Transl. Psychiat. *11*, 77. https://doi.org/10.1038/s41398-021-01202-3.

Podcasy, J.L., and Epperson, C.N. (2016). Considering sex and sex in Alzheimer disease and other dementias. Dialogues Clin. Neurosci. *18*, 437–446. https://doi.org/10.31887/DCNS.2016.18.4/cepperson.

Polis, B., and Samson, A.O. (2019). A new perspective on Alzheimer's disease as a brain expression of a complex metabolic disorder. In Alzheimer's Disease, T. Wisniewski, ed. (Brisbane (AU): Codon Publications).

Pollegioni, L., and Sacchi, S. (2010). Metabolism of the neuromodulator D-serine. Cell. Mol. Life Sci. *67*, 2387–2404. https://doi.org/10.1007/s00018-010-0307-9.

Punzo, D., Errico, F., Cristino, L., Sacchi, S., Keller, S., Belardo, C., Luongo, L., Nuzzo, T., Imperatore, R., Florio, E., et al. (2016). Age-related changes in D-aspartate oxidase promoter methylation control extracellular D-aspartate levels and prevent precocious cell death during brain aging. J. Neurosci. *36*, 3064–3078. https://doi.org/10.1523/JNEUROSCI.3881-15.2016.

Raber, J. (2004). Potential role of androgens and androgen receptors in Alzheimer's disease. In Alzheimer's Disease. Current Clinical Neurology, R.W. Richter and B.Z. Richter, eds. (Totowa, NJ: Humana Press). https://doi.org/10.1007/978-1-59259-661-4_30.

Rayaprolu, S., Higginbotham, L., Bagchi, P., Watson, C.M., Zhang, T., Levey, A.I., Rangaraju, S., and Seyfried, N.T. (2021). Systems-based proteomics to resolve the biology of Alzheimer's disease beyond amyloid and tau. Neuropsychopharmacology *46*, 98–115. https://doi.org/10.1038/s41386-020-00840-3.

Sacchi, S., Lorenzi, S., Molla, G., Pilone, M.S., Rossetti, C., and Pollegioni, L. (2002). Engineering the substrate specificity of D-amino-acid oxidase. J. Biol. Chem. *277*, 27510–27516. https://doi.org/10.1074/jbc.M203946200.

Sandusky-Beltran, L.A., Kovalenko, A., Placides, D.S., Ratnasamy, K., Ma, C., Hunt, J.B., Jr., Liang, H., Calahatian, J.I.T., Michalski, C., Fahnestock, M., et al. (2021). Aberrant AZIN2 and polyamine metabolism precipitates tau neuropathology. J. Clin. Invest. *131*, e126299. https://doi.org/10.1172/JCI126299.

Savarin, P., Barbet, A., Delga, S., Joshi, V., Hamon, L., Lefevre, J., Nakib, S., De Bandt, J.P., Moinard, C., Curmi, P.A., and Pastré, D. (2010). A central role for polyamines in microtubule assembly in cells. Biochem. J. *430*, 151–159. https://doi.org/10.1042/BJ20091811.

Schulte, C., Podestà, A., Lenardi, C., Tedeschi, G., and Milani, P. (2017). Quantitative control of protein and cell interaction with nanostructured surfaces by cluster assembling. Acc. Chem. Res. *50*, 231–239. https://doi.org/10.1021/acs.accounts.6b00433.

Sergin, I., Bhattacharya, S., Emanuel, R., Esen, E., Stokes, C.J., Evans, T.D., Arif, B., Curci, J.A., and Razani, B. (2016). Inclusion bodies enriched for p62 and polyubiquitinated proteins in macrophages protect against atherosclerosis. Sci. Signal. *9*, ra2. https://doi.org/10.1126/scisignal.aad5614.

Shaheen, R., Rahbeeni, Z., Alhashem, A., Faqeih, E., Zhao, Q., Xiong, Y., Almoisheer, A., Al-Qattan, S.M., Almadani, H.A., Al-Onazi, N., et al. (2014). Neu-Laxova syndrome, an inborn error of serine metabolism, is caused by mutations in PHGDH. Am. J. Hum. Genet. *94*, 898–904. https://doi.org/10.1016/j.ajhg.2014.04.015.

Simsir, I.Y., Soyaltin, U.E., and Cetinkalp, S. (2018). Glucagon like peptide-1 (GLP-1) likes Alzheimer's disease. Diabetes Metab. Syndr. *12*, 469–475. https://doi.org/10.1016/j.dsx.2018.03.002.

Smith, R., Strandberg, O., Mattsson-Carlgren, N., Leuzy, A., Palmqvist, S., Pontecorvo, M.J., Devous, M.D., Ossenkoppele, R., and Hansson, O. (2020). The accumulation rate of tau aggregates is higher in females and younger amyloid-positive subjects. Brain *143*, 3805–3815. https://doi.org/10.1093/brain/awaa327.

Sposato, V., Canu, N., Fico, E., Fusco, S., Bolasco, G., Ciotti, M.T., Spinelli, M., Mercanti, D., Grassi, C., Triaca, V., and Calissano, P. (2019). The medial septum is insulin resistant in the AD presymptomatic phase: rescue by nerve growth factor-driven IRS1 activation. Mol. Neurobiol. *56*, 3068. https://doi.org/10.1007/s12035-019-1525-2.

Szutowicz, A., Bielarczyk, H., Jankowska-Kulawy, A., Pawełczyk, T., and Ronowska, A. (2013). Acetyl-CoA the key factor for survival or death of cholinergic neurons in course of neurodegenerative diseases. Neurochem. Res. *38*, 1523–1542. https://doi.org/10.1007/s11064-013-1060-x.

Tripodi, F., Badone, B., Vescovi, M., Milanesi, R., Nonnis, S., Maffioli, E., Bonanomi, M., Gaglio, D., Tedeschi, G., and Coccetti, P. (2020). Methionine supplementation affects metabolism and reduces tumor aggressiveness in liver cancer cells. Cells *9*, 2491. https://doi.org/10.3390/cells9112491.

Tönnies, E., and Trushina, E. (2017). Oxidative stress, synaptic dysfunction, and Alzheimer's disease. J. Alzheimers Dis. *57*, 1105–1121. https://doi.org/10.3233/JAD-161088.

Tyanova, S., Temu, T., Sinitcyn, P., Carlson, A., Hein, M.Y., Geiger, T., Mann, M., and Cox, J. (2016). The Perseus computational platform for comprehensive analysis of (prote)omics data. Nat. Methods *13*, 731–740. https://doi.org/10.1038/nmeth.3901.

van Rooij, J.G.J., Meeter, L.H.H., Melhem, S., Nijholt, D.A.T., Wong, T.H., Netherlands Brain Bank; Rozemuller, A., Uitterlinden, A.G., van Meurs, J.G., and van Swieten, J.C. (2019). Hippocampal transcriptome profiling combined with protein-protein interaction analysis elucidates Alzheimer's disease pathways and genes. Neurobiol. Aging *74*, 225–233. https://doi.org/10.1016/j.neurobiolaging.2018.10.023.

Vizcaíno, J.A., Csordas, A., Del-Toro, N., Dianes, J.A., Griss, J., Lavidas, I., Mayer, G., Perez-Riverol, Y., Reisinger, F., Ternent, T., et al. (2016). 2016 update of the PRIDE database and its related tools. Nucleic Acids Res. *44*, 11033. https://doi.org/10.1093/nar/gkw880.

Wang, J., Tanila, H., Puoliväli, J., Kadish, I., and van Groen, T. (2003). Sex differences in the amount and deposition of amyloid beta in APPswe and PS1 double transgenic mice. Neurobiol. Dis. *14*, 318–327. https://doi.org/10.1016/j.nbd.2003.08.009.

Wang, C., Zhang, F., Jiang, S., Siedlak, S.L., Shen, L., Perry, G., Wang, X., Tang, B., and Zhu, X. (2016). Estrogen receptor-α is localized to neurofibrillary tangles in Alzheimer's disease. Sci. Rep. *6*, 20352. https://doi.org/10.1038/srep20352.

Wang, C., Wan, X., Yu, T., Huang, Z., Shen, C., Qi, Q., Xiang, S., Chen, X., Arbely, E., Ling, Z.Q., et al. (2020). Acetylation stabilizes phosphoglycerate dehydrogenase by disrupting the interaction of E3 ligase RNF5 to promote breast tumorigenesis. Cell Rep. *32*, 108021. https://doi.org/10.1016/j.celrep.2020.108021.

Wickens, M.M., Bangasser, D.A., and Briand, L.A. (2018). Sex differences in psychiatric disease: a focus on the glutamate system. Front. Mol. Neurosci. *11*, 197. https://doi.org/10.3389/fnmol.2018.00197.

Wolosker, H. (2011). Serine racemase and the serine shuttle between neurons and astrocytes. Biochim. Biophys. Acta *1814*, 1558–1566. https://doi.org/10.1016/j.bbapap.2011.01.001.

Wu, S.Z., Bodles, A.M., Porter, M.M., Griffin, W.S.T., Basile, A.S., and Barger, S.W. (2004). Induction of serine racemase expression and D-serine release from microglia by amyloid β-peptide. J. Neuroinflammation *1*, 2. https://doi.org/10.1186/1742-2094-1-2.

Xie, Y., Zheng, J., Li, S., Li, H., Zhou, Y., Zheng, W., Zhang, M., Liu, L., and Chen, Z. (2021). GLP-1 improves the neuronal supportive ability of astrocytes in Alzheimer's disease by regulating mitochondrial dysfunction via the cAMP/PKA pathway. Biochem. Pharmacol. *188*, 114578. https://doi.org/10.1016/j.bcp.2021.114578.

Yamazaki, D., Horiuchi, J., Ueno, K., Ueno, T., Saeki, S., Matsuno, M., Naganos, S., Miyashita, T., Hirano, Y., Nishikawa, H., et al. (2014). Glial dysfunction causes age-related memory impairment in *Drosophila*. Neuron *84*, 753–763. https://doi.org/10.1016/j.neuron.2014.09.039.

Yan, Z., Zhou, Z., Wu, Q., Chen, Z.B., Koo, E.H., and Zhong, S. (2020). Presymptomatic increase of an extracellular RNA in blood plasma associates with the development of Alzheimer's disease. Curr. Biol. *30*, 1771–1782.e3. https://doi.org/10.1016/j.cub.2020.02.084.

Yang, L., Garcia Canaveras, J.C., Chen, Z., Wang, L., Liang, L., Jang, C., Mayr, J.A., Zhang, Z., Ghergurovich, J.M., Zhan, L., et al. (2020). Serine catabolism feeds NADH when respiration is impaired. Cell Metab. *31*, 809–821.e6. https://doi.org/10.1016/j.cmet.2020.02.017.

Ye, J., Mancuso, A., Tong, X., Ward, P.S., Fan, J., Rabinowitz, J.D., and Thompson, C.B. (2012). Pyruvate kinase M2 promotes *de novo* serine synthesis to sustain mTORC1 activity and cell proliferation. Proc. Natl. Acad. Sci. USA *109*, 6904–6909. https://doi.org/10.1073/pnas.1204176109.

Zhang, Y., Li, P., Feng, J., and Wu, M. (2016). Dysfunction of NMDA receptors in Alzheimer's disease. Neurol. Sci. *37*, 1039–1047. https://doi.org/10.1007/s10072-016-2546-5.

Zhu, A., Ibrahim, J.G., and Love, M.I. (2019). Heavy-tailed prior distributions for sequence count data: removing the noise and preserving large differences. Bioinformatics *35*, 2084–2092. https://doi.org/10.1093/bioinformatics/bty895.

STAR★METHODS

KEY RESOURCES TABLE

REAGENT or RESOURCE	SOURCE	IDENTIFIER
Antibodies		
Rabbit polyclonal anti-PHGDH	Sigma	Cat#HPA024031; RRID:AB_1855300
Rabbit polyclonal anti-PSAT1 (anti-PSAT)	Antibodies online	Cat#abin2856767; RRID: AB_2923163
Rabbit polyclonal anti-PSPH (anti-PSP)	Invitrogen	Cat#PA5-22003; RRID:AB_11154135
Mouse monoclonal anti-GAPDH antibody	Thermo Fisher Scientific	Cat#MA5-15738; RRID:AB_10977387
Rabbit polyclonal anti-SR (home-made)	Davids Biotechnologie	N/A; RRID: AB_2923175
Rabbit polyclonal anti-DAAO	Abcam	Cat# ab187525; RRID: AB_2912164
Rabbit polyclonal anti-MPC1	Sigma	Cat# HPA045119; RRID: AB_10960421
Goat anti-rabbit IgG Alexa-Fluor Plus 800	Invitrogen	Cat#A32735; RRID:AB_2633284
IRDye 680RD Goat anti-Mouse IgG antibody	LI-COR Biosciences	Cat# 926-68070; RRID:AB_10956588
Biological samples		
Human brain samples (hippocampus) from male and female AD patients and healthy controls	Medical Research Council (MRC) London Neurodegenerative Diseases Brain Bank	N/A
Chemicals, peptides, and recombinant proteins		
TRIzol reagent	Invitrogen, Thermo Fisher Scientific	Cat#15596026
Urea	Sigma-Aldrich	Cat#U0631
Hepes	Sigma-Aldrich	Cat#H7523
cOmplete™, Mini Protease Inhibitor Cocktail	Roche	Cat#11836153001
Phosphatase Inhibitor Cocktail (100X)	Cell Signaling	Cat#5870
Dithioerythriol (1,4-dithioerythritol)	Sigma-Aldrich	Cat#D9680
Iodoacetamide	Sigma-Aldrich	Cat#I1149
Sequence Grade Modified Trypsin	Promega	Cat#V5111
Acetonitrile (ACN)	Sigma-Aldrich Carlo Erba	Cat#34851 Cat#75-05-8
Formic acid	Thermo Fisher Scientific	Cat#28905
Methanol LC-MS CHROMASOLV®	Honeywell - Riedel-de Haen®	Cat#34966
Methyl-tert-butyl ether (MTBE), CHROMASOLV™ Plus for HPLC, 99.9%	Honeywell - Riedel-de Haen®	Cat#650560
Reserpine	Supelco-Merck	Cat#43530
Methoxyamine hydrochloride 2% in pyridine, Methoxamine (MOX) Reagent	Thermo Fisher Scientific	Cat#TS-45950
N-methyl-N-(trimethylsilyl) trifluoroacetamid with 1% trimethylchlorosilane (MSTFA)	Supelco (Merck)	Cat#69478
d27-Myristic acid 0.75 mg/mL	Agilent	Cat#400505-54
EGTA	Sigma Aldrich	Cat#E3889
NP-40 - Tergitol	Sigma-Aldrich	Cat#NP40S
Tween-20	Sigma-Aldrich	Cat#93773
TCA - Trichloroacetic acid	Sigma-Aldrich	Cat#T9159
o-phthaldialdehyde	Sigma-Aldrich	Cat#P0657
N-acetyl L-cysteine	Sigma-Aldrich	Cat#A7250
Tetrahydrofuran	Carlo Erba	Cat#412451000
D-serine	Sigma-Aldrich	Cat#S4250
L-serine	Sigma-Aldrich	Cat#S4500
D-aspartic acid	Sigma-Aldrich	Cat#219096
L-aspartic acid	Sigma-Aldrich	Cat#11195

(*Continued on next page*)

Continued

REAGENT or RESOURCE	SOURCE	IDENTIFIER
Glycine	Sigma-Aldrich	Cat#G7126
Bradford reagent	BioRad	Cat#500-0205
M213R *Rhodotorula gracilis* D-amino acid oxidase (RgDAAO) variant	Sacchi et al., 2002	N/A
Critical commercial assays		
Trio RNA-Seq library kit-NuGEN	Tecan	Cat#0506
Agilent DNA 1000 Kit	Agilent	Cat#5067-1504
Agilent DNA 1000 Reagents	Agilent	Cat#5067-1505
Qubit™ dsDNA BR Assay Kit	Thermo Fisher Scientific	Cat#Q32850
Deposited data		
RNA-Seq data	This paper	NCBI SRA: PRJNA739253
Mass spectrometry proteomics data	This paper	PRIDE ProteomeXchange: PXD034137
Original western blot images	This paper	Mendeley: https://doi.org/10.17632/y8sp3489xt.2
Software and algorithms		
Novaseq sequencing control software	Illumina, Inc.	https://emea.support.illumina.com/sequencing/sequencing_instruments/novaseq-6000/downloads.htm
BCL2FASTQ v2.20 software	Illumina, Inc.	https://emea.support.illumina.com/downloads/bcl2fastq-conversion-software-v2-20.html
FASTQC software	Illumina, Inc.	https://www.bioinformatics.babraham.ac.uk/projects/fastqc/
STAR 2.7.3	Dobin and Gingeras, 2015	https://github.com/alexdobin/STAR/releases/tag/2.7.3a
Deseq2	Love et al., 2014	https://github.com/mikelove/DESeq2
apeglm package	Zhu et al., 2019	https://bioconductor.org/packages/apeglm
SALMON 0.13.1	Patro et al., 2017	https://github.com/COMBINE-lab/salmon/releases/tag/v1.3.0
tximportData	Love, 2022. R package version 1.24.0	https://bioconductor.org/packages/release/data/experiment/html/tximportData.html
DRIMSeq	Nowicka and Robinson, 2016	https://bioconductor.org/packages/release/bioc/html/DRIMSeq.html
ConsensusPathDB	Kamburov et al., 2009	http://cpdb.molgen.mpg.de
Ingenuity Pathway Analysis	Ingenuity® Systems	www.ingenuity.com
MaxQuant	Max-Planck-Institute of Biochemistry	https://www.maxquant.org/
Perseus	Max-Planck-Institute of Biochemistry	https://maxquant.net/perseus/
Panther	Thomas lab at the University of Southern California.	http://pantherdb.org/
DAVID	Laboratory of Human Retrovirology and Immunoinformatics (LHRI)	https://david.ncifcrf.gov/home.jsp
CLUEGO	Cytoskape	http://apps.cytoscape.org/apps/cluego
MetaboAnalyst	McGill Computational Structural & Systems Biology Lab	https://www.metaboanalyst.ca/
MassHunter	Agilent	
Image Studio	LI-COR	https://licor.app.box.com/s/4hrk823vov7vittqjg3onj51tb0wbo6w
Prism	Graphpad Software	https://www.graphpad.com/scientific-software/prism/

(*Continued on next page*)

Continued

REAGENT or RESOURCE	SOURCE	IDENTIFIER
Other		
NanoDrop 2000c	Thermo Fisher Scientific	Cat#ND-2000C
Agilent Bioanalyzer 2100	Agilent	Cat#G2939BA
Qubit 2.0 Fluorometer	Thermo Fisher Scientific	Cat#Q32866
®NovaSeq™6000 Sequencing System	Illumina	N/A
Dionex UltiMate 3000 RSLCnano LC System	Thermo Fisher Scientific	ULTIM3000RSLCNANO
Zip-Tip C18 - ™C18 Tips, 100 uL	Pierce	Cat#87784
Orbitrap Fusion Tribrid mass spectrometer	Thermo Fisher Scientific	IQLAAEGAAPFADBMBCX
Easy-Spray PepMap RSLC C18 column	Thermo Fisher Scientific	ES900
TissueLyser II	Qiagen	Cat# 85300
Vacufuge plus	Eppendorf	Cat# EP022822993
1290 Infinity UHPLC system	Agilent	N/A
InfinityLab Poroshell 120 PFP column	Agilent	Cat#695775-408
6550 iFunnel Q-TOF mass spectrometer	Agilent	N/A
Sample Prep WorkBench	Agilent	Cat#7696A
DB-35MS column	Agilent	Cat#122-3832UI-INT
Intuvo 9000 GC System	Agilent	N/A
Mini Trans-Blot Electrophoretic Transfer Cell	BIO RAD	Cat# 1703930
Odyssey Fc	LI-COR	N/A
HPLC apparatus LC-2000Plus (PU-2089Plus Quaternary low pressure gradient pump, CO-2065 column oven, FP-2020 fluorescence detector, AS-2059 autosampler)	Jasco	N/A
Symmetry C8 reversed-phase column	Waters	Cat#WAT054270

RESOURCE AVAILABILITY

Lead contact

Further information and requests for resources and reagents should be directed to and will be fulfilled by the lead contact, Silvia Sacchi (silvia.sacchi@uninsubria.it).

Materials availability

This study did not generate new unique reagents.

Data and code availability

- RNA-seq raw data reported in this paper have been deposited at NCBI SRA and are publicly available as of the date of publication. The BioProject ID is listed in the key resources table. Mass spectrometry proteomics data have been deposited to the ProteomeXchange Consortium via the PRIDE partner repository. The dataset identifier is listed in the key resources table. Original Western blot images have been deposited at Mendeley and are publicly available as of the date of publication. The DOI is listed in the key resources table. All metabolomics data reported in this paper will be shared by the lead contact upon request.
- This paper does not report original code.
- Any additional information required to reanalyze the data reported in this paper is available from the lead contact upon request.

EXPERIMENTAL MODEL AND SUBJECT DETAILS

Patient cohorts and brain samples

Control (CTR) and Alzheimer's disease (AD) brain samples (hippocampus) were obtained from the Medical Research Council (MRC) London Neurodegenerative Diseases Brain Bank hosted at the Institute of Psychiatry, Psychology and Neuroscience, KCL. All cases were collected under informed consent, and the bank operates under a licence from the Human Tissue Authority, and ethical approval as a research tissue bank (08/MRE09/38+5). Neuropathological evaluation for neurodegenerative diseases was performed in accordance with standard criteria. All methods were carried out in accordance with relevant guidelines and regulations and the study was approved by the Institutional Review Board of the University of Rome "Tor Vergata" (Protocol N°98.18). All sampled individuals were European; men and women showed a comparable age of death (Mann-Whitney test >0.5).

The age distribution of CTR samples was in the 81.2±4.9 range (mean ± SD) with PMI intervals included between 3 and 48 h (Table S1). All CTR samples derived from both female and male patients that were classified as normal brains with minimal ageing changes (Table S1). Similar age distribution was obtained for AD samples (82.8±5.9), with PMI intervals included between 4 and 20.5 h (Table S1). Details of each sample are described in Table S1. Considering sex separation: CTRF: n = 12, age distribution = 81.2 ± 5.25, 3 < PMI<35 hours; CTRM: n = 9, age distribution 81.3 ± 4.8, 6 < PMI<48 hours; ADF: n = 15, age distribution 85.1 ± 4.5, 4 < PMI<13; ADM: n = 12, age distribution 80.0 ± 6.45, 5.25 < PMI<20.5. CTRs were defined as having no evidence of dementia, i.e. donors with minimal aging changes, mild cognitive impairment and neuropathological findings insufficient to meet criteria for AD. All patients with AD had Braak stages in the range of IV-VI. Tissue samples of 500–1000 mg were dissected and stored at −80°C until analysis.

METHOD DETAILS

RNA extraction, libraries, and sequencing

Total RNA was extracted using TRIzol reagent (Invitrogen, Thermo Fisher Scientific) following the manufacturer's protocol from CTR and AD samples (Table S1). Both CTRL and AD samples have comparable age (82.40 ± 2.02 vs 86.43 ± 2.10; Mann Whitney test = 0.32) and PMI (12.40 ± 4.10 vs 10.93 ± 0.94; Mann Whitney test = 0.93). RNA was quantitatively and qualitatively evaluated using NanoDrop 2000c (Thermo Fisher Scientific) and Agilent Bioanalyzer 2100 (Agilent), respectively. RNA-seq libraries were prepared from 1 μg of total hippocampal RNA, using the Trio RNA-Seq library kit-NuGEN (Tecan) according to the manufacturer's protocol. The Nugen system is optimised for the amplification of low input amounts RNA, where amplification is initiated at the 3′ end as well as randomly throughout the whole transcriptome. cDNA libraries were checked on a DNA 1000 Chip using the corresponding reagents (Agilent DNA 1000 Kit) and the Bioanalyzer 2100 (Agilent) and quantified using Qubit™ dsDNA BR Assay Kit on Qubit 2.0 Fluorometer (Thermo Fisher Scientific). Sequencing was performed on ®NovaSeq™6000 Sequencing System (Illumina, Inc), generating for each sample almost 40 million of 2x150 bp paired-end reads.

RNA sequencing was performed at CBM Scrl (Consorzio per il Centro di Medicina Molecolare) Area Science Park, Basovizza, Trieste (Italy).

Preprocessing and analysis of RNA-seq data

Real-time image analysis and base calling were performed directly on the Novaseq instrument using the recommended sequencing control software. Illumina BCL2FASTQ v2.20 software was used for de-multiplexing and production of FASTQ sequence files. FASTQ raw sequence files were subsequently quality checked with FASTQC software. Subsequently, sequences with a low-quality score Q<20 or including adaptor dimers or mitochondrial or ribosomal sequences, were discarded from the analysis. The resulting set of selected reads were aligned onto the complete human genome using Spliced Transcripts Alignment to a Reference algorithm STAR version 2.7.3 (Dobin and Gingeras, 2015) using hg38 Genome Assembly and Gencode.v26 as gene definition. The resulting Mapped reads were used as input for feature Counts function of Rsubread packages and used as Genes counts for differentially expression analysis using Deseq2 package (Love et al., 2014). We used the shrinkage estimator from the apeglm package (Zhu et al., 2019) for visualization and ranking.

Original FASTQ files have been aligned against hg38 by means of SALMON version 0.13.1 (Patro et al., 2017) against all 57,820 gene features in gencode.v26.pc_transcripts (Liao et al., 2014). Pondering 10 as the lowest number of reads to map a given gene, RNA-seq data analysis identified 20689 annotated genes as expressed in all sequenced samples. Transcript levels have been loaded in R environment using tximportData package while differential transcript usage (DTU) has been evaluated using DRIMSeq package (Nowicka and Robinson, 2016). DTU analysis, a measure of the relative contribution of one transcript to the overall expression of the gene (i.e. the total transcriptional output) based on individual transcript read counts normalized to the sum of all transcript read counts of the gene, was used to characterize differences in the isoform landscape of *PHGDH*, *PSAT*, *PSP*, *SR*, and *DAAO*. The RNA seq data has been deposited to the SRA repository with the BioProject identifier PRJNA739253.

To compare our transcriptome analysis with other published data (since not all published data are available), we used the fry function of the package EdgeR for a Rotation Gene Set test creating a gene sets starting from tables of DEGs available in the two papers reported (Crist et al., 2021, PMID_33875655; Mathys et al., 2019, PMID_31042697).

Mass-spectrometry-based proteomics analysis

Human hippocampus proteome from control patients (9 men and 10 women) and patients with AD (10 men and 10 women) was analyzed by a shotgun label free proteomic approach for the identification and quantification of expressed proteins. Approximately 20 mg of brain tissues from each subject were homogenized using a Potter homogenizer in 100 μL of extraction buffer (8 M urea, 20 mM Hepes pH 8.0, with Protease and Phosphatase Inhibitors cocktail) at full speed for 1 min as previously reported in (Nonnis et al., 2016). The homogenate was sonicated using an ultrasonic probe in bursts of 20–30 s and centrifuged at 16060 × g for 15 min at 18°C to pellet the tissue debris. Prior to proteolysis, proteins were reduced with 13 mM dithioerythriol (30 min at 55°C) and alkylated with 26 mM iodoacetamide (30 min at room temperature). Protein digestion was performed using sequence-grade trypsin (Promega) for 16 h at 37°C using a protein: enzyme ratio of 20:1. The collected peptides were desalted using Zip-Tip C18 before Mass Spectrometric (MS) analysis as reported in (Galli et al., 2018). NanoHPLC coupled to MS/MS analysis was performed

on Dionex UltiMate 3000 directly connected to an Orbitrap Fusion Tribrid mass spectrometer (Thermo Fisher Scientific) by a nano-electrospray ion source. Peptide mixtures were enriched on 75 μm ID × 150 mm EASY-Spray PepMap RSLC C18 column (Thermo Fisher Scientific) and separated using the LC gradient: 1% acetonitrile (ACN) in 0.1% formic acid for 10 min, 1–4% ACN in 0.1% formic acid for 6 min, 4–30% ACN in 0.1% formic acid for 147 min and 30–50% ACN in 0.1% formic for 3 min at a flow rate of 0.3 μL/min. Orbitrap-MS spectra of eluting peptides were collected over an m/z range of 375–1500 at resolution of 120,000, operating in a data-dependent mode with a cycle time of 3 s between master scans. HCD MS/MS spectra were acquired in Orbitrap at resolution of 15,000 using a normalized collision energy of 35%, and an isolation window of 1.6 m/z. Dynamic exclusion was set to 60 s. Rejection of +1, and unassigned charge states were enabled.

The mass spectrometry proteomics data have been deposited to the ProteomeXchange Consortium via the PRIDE (Vizcaíno et al., 2016) partner repository.

Metabolites extraction

For LC-MS analyses, 200 μL ice-cold 50:50 methanol-water were added to 20 mg of frozen tissue and samples were homogenized in a bead mill (TissueLyser II, Qiagen) with stainless steel beads (5 mm) for 1 min, 30 Hz power. After a 30 min incubation at −80°C, 100 μL of homogenate was vortexed with 320 μL of ice-cold methanol for 2 min. Then, 80 μL of methyl-tert-butyl ether (MTBE) was added and samples were placed in a thermoshaker for 1 h at 4°C.

On the other hand, for GC-MS analyses 400 μL ice-cold 50:50 methanol-water was added to the same amount of frozen tissue (20 mg) and samples were homogenized and incubated at −80°C as above. Then, samples were centrifuged at 12,000 g for 10 min at 4°C. 400 μL of ice-cold chloroform was added and samples were placed in a thermoshaker for 1 h at 4°C.

In both cases, extracted samples were subsequently centrifuged at 12,000 g for 10 min at 4°C. 400 μL of supernatant was collected in a glass insert and dried in a centrifugal vacuum concentrator (Concentrator plus/Vacufuge plus, Eppendorf) at 30°C for about 2.5 h. Samples for LC-MS analysis were then resuspended in 150 μL of H_2O prior to analyses, whereas samples for GC-MS analysis were subjected to derivatization as detailed below.

Metabolic profiling

LC separation during LC-MS analyses was performed using an Agilent 1290 Infinity UHPLC system and an InfinityLab Poroshell 120 PFP column (2.1 × 100 mm, 2.7 μm; Agilent). Mobile phase A was water with 0.1% formic acid. Mobile phase B was ACN with 0.1% formic acid. The injection volume was 15 μL and LC gradient conditions were: 0 min: 100% A; 2 min: 100% A; 4 min: 99% A; 7 min: 98%; 8 min: 70% A; 10 min: 70% A; 13 min: 30% A; 15 min: 30% A; 16 min: 100% A; 18 min: 100% A with 2 min of post-run. Flow rate was 0.2 mL/min and column temperature was 35°C. MS detection was performed using an Agilent 6550 iFunnel Q-TOF mass spectrometer with Dual JetStream source operating in negative ionization mode. MS parameters were: gas temperature: 285°C; gas flow: 14 L/min; nebulizer pressure: 45 psig; sheath gas temp: 330°C; sheath gas flow: 12 L/min; VCap: 3700 V; Fragmentor: 175 V; Skimmer: 65 V; Octopole RF: 750 V. Active reference mass correction was performed through a second nebulizer using masses with m/z: 112.9855 and 1033.9881 dissolved in the mobile phase 2-propanol-ACN-water (70:20:10 v/v) at a flow rate of 0.15 mL/min. Data were acquired from m/z 60 to 1050.

For GC-MS analyses, derivatization was performed using an automated sample prep WorkBench instrument (Agilent). Dried polar metabolites were dissolved in 60 μL of 2% methoxyamine hydrochloride in pyridine and held at 40°C for 6 h. After the reaction, 90 μL of N-methyl-N-(trimethylsilyl) trifluoroacetamid (MSTFA) was added and samples were incubated at 60°C for 1 h. Derivatized samples were analyzed by GC-MS using a DB-35MS column (30 m × 0.25 mm, i.d. x 0.25 μm; Agilent) installed in an Agilent Intuvo 9000 gas chromatograph interfaced with a 5977B mass spectrometer operating under electron impact (EI) ionization at 70 eV. Samples (1 μL) were injected in a splitless mode at 250°C, using helium as the carrier gas at a flow rate of 1 mL/min. The GC oven temperature was held at 100°C for 2 min and increased to 325°C at 10°C/min.

The metabolic analyses were carried out in outsourcing by the ISBE.IT/Center of Systems Biology, Milan, Italy.

Western blot analysis

Brain samples were homogenized in 20 mM HEPES pH 8.0, 1 mM EGTA, 0.4% NP-40, and added of complete protease- (Roche) and phosphatase-inhibitor (Cell Signaling) cocktails, prepared following the manufacturer's instructions, (100 μL for 10 mg of tissue), using a pellet micro-pestle and then subjected to sonication (3 cycles, 20 s each). The lysates were centrifuged at 13,000 × g for 10 min at 4°C and, after discarding the pellet, the concentration of total proteins in the supernatant was determined using the Bradford reagent (BioRad). For each sample 40 μg of total proteins were subjected to SDS-PAGE and transferred on a PVDF membrane using the Mini Trans-Blot Cell system (BioRad). The membranes were developed using rabbit anti-PHGDH (Sigma-Aldrich), anti-PSAT (Antibodies online), anti-PSP (Invitrogen), anti-SR (Davids Biotechnologie), anti-DAAO (Abcam) and anti-MPC1 (Sigma-Aldrich) antibodies. The membrane was blocked overnight at 4°C with 4% dried milk in Tris-saline buffer pH 8.0 added of 0.1% Tween 20 and subsequently incubated with primary antibodies, the anti-SR diluted 1:10, the anti-MPC1 diluted 1:500 all the others diluted 1:1000 in 2% dried milk in Tris-saline buffer pH 8.0 added of 0.05% Tween 20 overnight at 4°C for the anti-MPC1 and for 2 h at room temperature for all the others. After extensive washing, the membrane was incubated for 1 h at room temperature with goat anti-rabbit IgG (Alexa-Fluor Plus 800 Invitrogen, 1:20,000 dilution in Tris-saline buffer pH 8.0 added 0.05% Tween 20). Western blots were analyzed by an Odyssey Fc apparatus equipped with the ImageStudio software (LI-COR Biosciences): the intensity signal of

each sample was normalized by the GAPDH signal (detected using a mouse anti-GAPDH antibody, 1:2000, Thermo Fisher Scientific; and a goat anti-mouse IgG IRDye 680RD, 1:5000, LI-COR Biosciences). The content of each protein was calculated by the software based on the intensity of known amounts of recombinant proteins and was related to the μg of total proteins loaded into the gel. Controls included the addition of a known amount (10 ng PHGDH and PSAT and 2.5 ng PSP) of recombinant proteins to the samples. Each sample was analyzed at least three times (in three different SDS-PAGE runs).

Enantiomeric HPLC analysis

Brain tissue samples were analyzed using the procedure reported in (Punzo et al., 2016) with minor modifications. Samples were homogenized in 1:10 (w/v) 0.2 M TCA, sonicated (three cycles of 10 s each), and centrifuged at 13,000 × g for 20 min at 4°C. The precipitated protein pellets were stored at −80°C for quantification, and 10 μL of the supernatants were neutralized with NaOH and subjected to precolumn derivatization with 20 μL of 74.5 mM *o*-phthaldialdehyde and 30.5 mM N-acetyl L-cysteine in 50% methanol. Diastereoisomer derivatives were then resolved on a Symmetry C8 reversed-phase column (5 μm, 4.6 × 250 mm, Waters) under isocratic conditions (0.1 M sodium acetate buffer, pH 6.2, 1% tetrahydrofuran, at 1 mL/min flow rate). A washing step in 0.1 M sodium acetate buffer, 3% tetrahydrofuran and 47% ACN was performed after each run. Identification and quantification of D- and L-Ser, D- and L-Asp, and Gly were based on retention times and peak areas, compared with those associated with external standards. The identity of D-Ser and D-Asp peaks was further confirmed by adding known amounts of external standards and by their selective degradation using wild-type or M213R RgDAAO variant, respectively (Sacchi et al., 2002). The enzymatic treatment allowed a more precise estimation of the amino acid concentration: the samples were added with 10 μg of the enzymes (approx. 600 and 60 mU for wild-type and M213R RgDAAO, respectively), incubated at 30°C for 60 min and then derivatized. The amino acids total amount detected in homogenates was normalized by grams of tissue.

QUANTIFICATION AND STATISTICAL ANALYSIS

RNA-seq data analysis

DESeq2 uses a generalized linear model to evaluate differential expression while accounting for biological variance and uses a Wald test statistic to estimate significance. The Principal Component Analysis (PCA) was calculated using "prcomp" in R on gene expression values obtained by DEseq2 on RNA-seq aligned reads after removing the sex effect via the Sva package. DEGs with $|Log2(FC)| \geq 1$ and adjusted p value ≤ 0.05 were used as input to perform Gene Set Enrichment Analysis (GSEA) and pathway enrichment analysis. GSEA was performed using Over-Representation Analysis (ORA) of the ConsensusPathDB functional interaction database (Kamburov et al., 2009). ConsensusPathDB includes several known biological pathway databases including KEGG, BioCarta, Reactome, and Wikipathways. It performs a hypergeometric test while relating a background gene list, assembles results from each database and corrects for multiple testing using (false discovery rate) FDR (Kamburov et al., 2009). GSEA analysis was performed setting at 2 the minimum overlap between the query signature and database. Pathway enrichment analysis was also performed by Ingenuity Pathway Analysis (IPA) (Ingenuity Systems). DRIMseq, used to identify differential transcript usage, is based on modeling the counts of transcripts with the Dirichlet-multinomial distribution.

Label-free proteomics

A database search was conducted against the *Homo sapiens* Uniprot sequence database (https://www.uniprot.org/proteomes, released 9 January 2020) with MaxQuant (version 1.6.1.0) software. The initial maximum allowed mass deviation was set to 10 ppm for monoisotopic precursor ions and 0.5 Da for MS/MS peaks. Enzyme specificity was set to trypsin, defined as C-terminal to Arg and Lys excluding Pro, and a maximum of two missed cleavages were allowed. Carbamidomethylcysteine was set as a fixed modification, while N-terminal acetylation, Met oxidation, Asn/Gln deamidation and Ser/Thr/Tyr phosphorylation were set as variable modifications. Quantification in MaxQuant was performed using the built-in label free quantification algorithms (LFQ) based on extracted ion intensity of precursor ions. False protein identifications (1%) were estimated by searching MS/MS spectra against the corresponding reversed-sequence (decoy) database. Statistical analysis was performed using the Perseus software (version 1.5.5.3) (Tyanova et al., 2016). Only proteins present and quantified in at least 80% of the repeats were positively identified in a sample and used for statistical analysis. Focusing on specific comparisons, proteins were considered differentially expressed if they were present only in one condition or showed significant t test difference (Student's t-test p value ≤ 0.05) (Schulte et al., 2017).

Bioinformatic analyses were carried out by Panther software (release 16.0) (Mi et al., 2013), DAVID software (release 6.8) (Huang et al., 2009) and CLUEGO software (Cytoskape release 3.8.2) (Bindea et al., 2009) to cluster enriched annotation groups of Biological Processes, Pathways, and Networks within the set of identified proteins. Functional grouping was based on Fischer's exact test p value ≤ 0.05 and at least 3 counts. Integration between proteomic and metabolomics data was performed by MetaboAnalyst software R5.0 based on a Fischer's exact test p value ≤ 0.05 (Tripodi et al., 2020). The topology analysis aimed to evaluate whether a given gene or metabolite plays an important role in a biological response, based on its position within a pathway (pathway impact).

Metabolic profiling

LC-MS data analysis and isotopic natural abundance correction was performed with MassHunter ProFinder (Agilent). Relative metabolite abundance was carried out after normalization to internal standard reserpine.

GC/MS data processing was performed using Agilent Mass Hunter software. Relative metabolite abundance was carried out after normalization to internal standard d27-myristic acid. Statistical analyses were performed using MetaboAnalyst 5.0, p value $\leq$ 0.05 (Chong et al., 2019).

Western blot analysis

The results were analyzed using GraphPad Prism version 7.0 for Windows (GraphPad Software). The D'Agostino and Pearson normality test was used to analyze the distribution of variables: since a non-normal distribution was observed, a non-parametric approach was used for all statistical analyses. Variation of protein levels between controls and AD patients was evaluated using the two-tailed Mann-Whitney test. A p value < 0.05 was considered as statistically significant.

Enantiomeric HPLC analysis

All statistical analyses were performed using GraphPad Prism 7.0. Distribution of the values of variables was assessed by the D'Agostino and Pearson or Shapiro-Wilk (for sex comparison) normality tests. Since not all groups showed Gaussian distribution, analyses were performed using the non-parametric two-tailed Mann–Whitney test. A p value lower than 0.05 was considered statistically significant. In all statistical analyses, one outlier in the dataset of the female control group was excluded.